Politecnico di Torino

Non-linear Model Predictive Controller for the autonomous descent and landing of a parafoil system in multi-planetary applications

Candidate
Michele Gasparri

Supervisor
Prof. Carlo Novara

Thesis for Master's degree in
Mechatronics Engineering

Dipartimento di Elettronica e Telecomunicazioni
Politecnico di Torino

28 Luglio 2023

Abstract

The objective of this thesis is to evaluate the applicability of a non-linear Model Predictive Controller in multi planetary environments for control of an autonomous parafoil system.
The work stems from many examples of the use of parafoils and parachute as a landing system on planets with suitable atmospheric conditions. As in terrestrial applications, from the thrill of paragliding to the need of deploying resources to the battlefield, or in space exploration where landing critical instruments on a planet leaves no room for error, parafoils have always been explored as a possible solution.
Focusing on implementing a simulation environment able to correctly represent the dynamics of the system at hand and the different environments considered. The data generated is used in the system identification of the reduced order models employed in the controller. The controller parameters are tuned using a weight scheduling technique, to allow for the different required behaviour during the descent of the system and optimized for each environment. Finally, the performance is analysed in different atmospheric conditions, obtaining information on the critical aspects of the application.
Scenarios for the simulations differ for each planetary application, as the atmospheric modellization and the parameters that are relevant for the analysis. For Earth, a wind disturbance parametrized as a fraction of the planar velocity of the system is considered, as to generate a significant disturbance which is still manageable for the controller. On Mars a constant wind disturbance is considered, aligning this work to the other studies present in literature. On Titan, an exponential parametrization of the wind is employed, stemming from the research carried out by NASA with the Huygens spacecraft.
The obtained results are comparable to other techniques for the application on Earth and on Mars, while the performance on Titan is adequately better than studies previously carried out in this field.

Contents

List of Figures

Chapter 1

Introduction

1.1 Research context and related works

Planetary and interplanetary logistics is one of the most complex problems that we, as a species, have faced. Delivering resources to far away places is already complex when 347 million kilometres of void are not standing in between. Exploring other planet has always been a milestone for researchers all around the world. Currently we've landed on three: Venus, Titan, and Mars. Just three out of the more than five thousand planets known to man. There is still a lot to explore, and even more that we don't know the existence of.

Reaching these planets is still an achievement, even leaving planet earth reliably is an achievement in itself. Thus, it is of paramount importance to be able to successfully land anything that we can get close enough to do so. This final operation is subject to many constraints. From the initial velocity, which may damage or otherwise disable the landing vector. To the landing accuracy and reliability, because even if reaching America has proven a lucrative endeavour, imagine what would have happened if Colombo really reached India.

During the entry and descent phases of approach towards the surface of a planet, a lot of kinetic energy must be shedded. The Huygens mission to Titan employed an entry strategy with a first deceleration provided by coni-spherical descent shield followed by three different parachute stages. One supersonic, one from the transonic range to subsonic velocities, and one final stabilizer for the subsonic descent and landing[1].

The applicability of parachutes, being them disk gap band or ram-air aerofoils, is strictly dependent on the atmospheric and environmental conditions[2][3]. A suitable balance of atmospheric density, acceleration of gravity and wind conditions must be present for a successful descent and landing. Making this type of final approach very environment dependent. Moreover, Titan's high atmospheric density results in a slow entry, descent, and landing (EDL) phase, allowing ample time for significant changes in wind profiles[4]. On the other hand, a parachute is technically less complex than a thruster-based landing vector. Being intrinsically stable[5] and easier to control, it provides a less complex solution to a very difficult problem. Energy expenditure is lowered, and the dynamics are much slower, allowing for control algorithms to run at a lower frequency.

To solve the control problem, most research project employed in simulation proportional-derivative control [3] and proportional control coupled with optimal-trajectory planning [6]. More complex approaches employ "pseudo-optimal" control inspired by human manoeuvring [7], or dynamic programming for the trajectory generation coupled with a model predictive controller [4]. Still, apart from this last instance, the writer of this paper is not aware of any real effort to develop a guidance, control and navigation system for planetary exploration that is designed and optimized for parafoils.

1.2 Objectives

The objective of this thesis is to explore a non-linear Model Predictive Controller (n-MPC), with adaptive capabilities, as the sole player in the control of the system. This involves developing and implementing the n-MPC control strategy, developing the simulation environment, and estimating the reduced order model's parameter for the controller prediction. Evaluating the controller's performance in terms of achieving desired objectives, such as accurate landing, energy efficiency, and minimizing deviations from the desired trajectory.
The mentioned system is a parafoil with payload, which refers to the combination of a parafoil canopy and a payload attached to it. The dimensions and aerodynamic characteristics of the parafoil vary depending on the specific application.
As stated above, the objective is to explore multiple environment ap-

plication for this control approach. Here follows a brief overview and comparison of the characteristics and difficulties found in each considered environment.

- Earth's atmosphere provides a favourable environment for parafoil operations due to its relatively high atmospheric density, moderate wind speeds, and well-understood atmospheric conditions. The performance of parafoils on Earth is influenced by factors such as atmospheric pressure, temperature, wind speed, and local topography.
- Mars has a much thinner atmosphere compared to Earth, with significantly lower atmospheric density. This poses challenges for parafoil operations, as the reduced density affects the generation of lift and overall performance. The lower gravity on Mars is an advantage, as it allows for slower descent rates. However, the limited atmospheric density and the potential for strong winds on Mars need to be carefully considered in parafoil design and mission planning.
- Titan, one of Saturn's moons, has a unique atmosphere composed mainly of nitrogen with traces of methane. Its atmospheric density is considerably higher than that of Mars but still much lower than Earth's. The lower gravity on Titan allows for gentle descents, but the specific atmospheric conditions, including the presence of an organic haze and occasional storms, need to be accounted for in parafoil and mission design.

Simulating this control approach in different environments allows to evaluate the flexibility of this type of solution, evaluate its weaknesses, and provides better understanding of the different behaviours that can be obtained.

1.3 Contribution and results

To realize what stated above, a simulation environment was developed in Simulink, encompassing a 6 degrees-of-freedom model of the system, atmospheric conditions for the different planetary applications, variable wind disturbances and initial conditions. The simulation environment was used both in the estimation of the reduced order model

parameters and in the Monte Carlo simulations for the evaluation of the performance of the controller.
Specifically, the project was carried out along the following topics:

- **Study and implementation of the dynamic model of the parafoil system.** While implementing in a simulation environment the dynamic equations of a system is usually a straight forward endeavour, in the case of parafoil system a lot of incomplete information is found in literature. Thus a lot of time was initially spent on finding a complete model and all the relative parameters to correctly describe the system. The six degrees-of-freedom model was chosen to describe the dynamics, as it is found in many different works. Allowing for a simple simulation framework that can be employed in all the different planetary applications.
  For the prediction model, the four dof model was chosen above a three dof model. The choice is motivated by the dual input of the first, compared to the single input of the latter. Allowing for further flexibility in the control of the system.

- **Identification of the reduced order model parameters.** A methodology was developed to obtain valid data, whilst considering the computational complexity that this problem poses. The final results are far from perfect, from a numerical stand-point, but yield sufficiently good performance in the simulations, evidence of the flexibility of the control strategy employed.

- **Development and tuning of the n-MPC controller.** The base formulation of the non-linear Model Predictive Controller was taken from previous works but didn't demonstrate to be sufficiently robust and adaptable to the problem at hand. The act of scheduling of the optimization weight pertaining to the control effort, previously found only in wind turbines, proved to be highly effective at tackling the numerical variance of the input variables of the objective function.

Many factors concur to the final performance of the controller, from the identification of the reduced order models parameters, the tuning of the controller, to the atmospheric conditions. In all cases, the results of the simulations show how the controller can correctly perform under generally nominal atmospheric conditions. Considering the dispersion of the landing points as a bivariate gaussian distribution, the values of the semi-axis of the error ellipses calculated for a 90% likelihood are comparable with other works done in the field of planetary exploration. Furthermore, the controller is able to follow trajectories that are not spiraling, but present straight passes with seldom direction changes. This represents an advantage from both a stability and energy expenditure perspective.

Compared to controllers where a complete descent trajectory is calculated, the controller achieves similar levels of accuracy, while being less complex and more open to implementation of disturbance identification and rejection strategies. The results achieved place this solution, a non-linear Model Predictive Controller with scheduled optimization weights, as a good candidate for the control of parafoils in the final stages of planetary descent and landing. Limitations on the applicability of this strategy are mainly due to the system itself, than from the controller's performance.

Chapter 2

Mathematical models

2.1 Reference frames and Rotation

The dynamics and kinematics of a parafoil system require the use of multiple reference frames to accurately describe and organize the system's behavior. These reference frames are associated with the main components of the system that experience forces during the flight. The reference frames help in understanding and analyzing the forces and motions involved.
The following are the reference frames employed in the analysis of parafoil system.

Planet reference frame

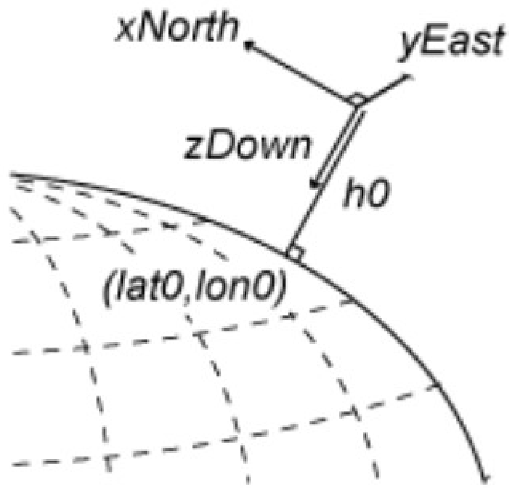

Figure 2.1: NED reference frame

Responsible for identifying the absolute position in space, it is oriented as NED - North East Down - figure 2.1. In the following text it will be referred to as $\{i\}$.

- Origin: Arbitrary point on the surface.
- x axis: Aligned with the north-south axis, pointing North.
- y axis: Aligned with the west-east axis, pointing East.
- z axis: Perpendicular to the x and y axes, pointing toward the center planet.

Body reference frame

The body reference frame is rigidly fixed with the body, and is fundamental for defining the pose in space. Hereafter referred to as $\{b\}$.

- Origin: CoM of the body.
- x_b axis: Positive out of the longitudinal axis, on the vertical plane of symmetry.
- z_b axis: Perpendicular to x_b, in the vertical plane of symmetry. Positive going from the canopy to the payload.
- y_b axis: Perpendicular to x_b and z_b, positive direction given by the right-hand rule.

Wind reference frame

Also referred to as $\{w\}$.

- Origin: CoM of the body..
- x_w axis: Positive in the direction of the velocity $\boldsymbol{V_a}$ relative to the atmosphere.
- z_w axis: Perpendicular to x_w in the vertical plane of symmetry. Positive going from the canopy to the payload.
- y_w axis: Perpendicular to x_w and z_w, positive direction given by the right-hand rule.

Additional reference frames

In addition to the aforementioned reference frames, two other are useful to correctly develop the mathematical context for the model [3]: *Navigational* reference frame and *Canopy* reference frame. Also referred to as $\{n\}$, the navigational reference frame is parallel to {i}, but centered in the body CoM. The canopy reference frame is centred in the apparent mass center, and is rotated by a negative angle μ, around the y_b axis, with respect to $\{b\}$.

2.1.1 Angles and Rotation matrices

Basic angle definitions

- ψ: Yaw - From the North to the x_b axis, in the horizontal plane.
- θ: Pitch - From the horizontal plane to the longitudinal axis x_b.
- ϕ: Roll - Formally is defined as the rotation along the longitudinal axis of the craft. In our case, it is the angle that completes the rotation from $\{n\}$ to $\{b\}$.
- α: Angle of attack - From the projection of $\boldsymbol{V_a}$ on to $\vec{z_b} \times \vec{x_b}$ to the longitudinal axis x_b.
- β: Side slip angle - From $\boldsymbol{V_a}$ to its projection on the $\vec{z_b} \times \vec{x_b}$.
- μ: Rigging angle - Rotation of p with-respect-to b, around the y direction. It is a negative angle.

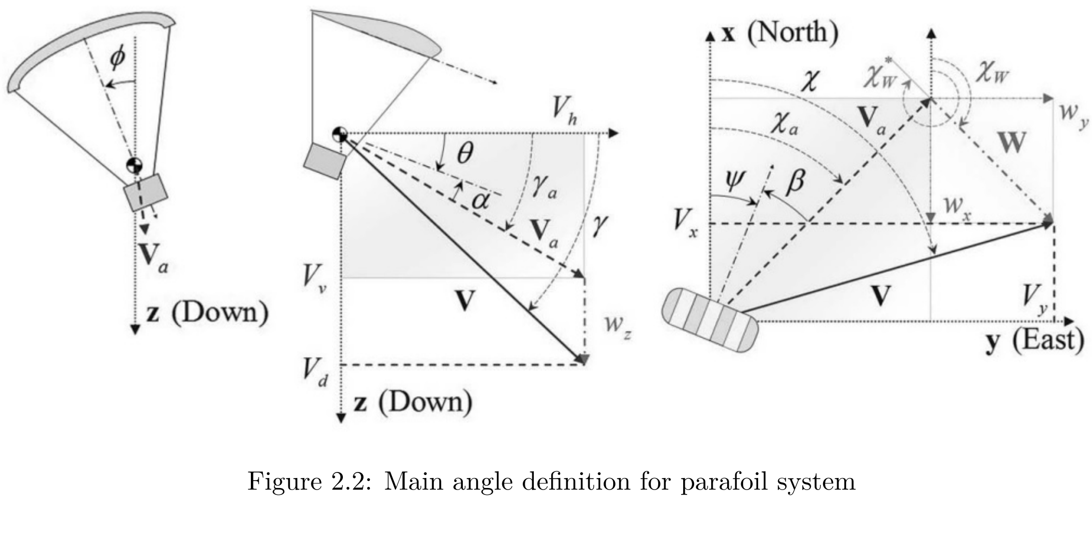

Figure 2.2: Main angle definition for parafoil system

Rotation matrices

All of the the rotation matrices follow the Euler Angles composition rules, and are based on the basic rotation matrices[3][8][6].

$$\boldsymbol{R_i}(x) = \begin{bmatrix} 1 & 0 & 0 \\ 0 & \cos x & -\sin x \\ 0 & \sin x & \cos x \end{bmatrix} \tag{2.1}$$

$$\boldsymbol{R_j}(x) = \begin{bmatrix} \cos x & 0 & \sin x \\ 0 & 1 & 0 \\ -\sin x & 0 & \cos x \end{bmatrix} \tag{2.2}$$

$$\boldsymbol{R_k}(x) = \begin{bmatrix} \cos x & -\sin x & 0 \\ \sin x & \cos x & 0 \\ 0 & 0 & 1 \end{bmatrix} \tag{2.3}$$

Thus using the pre-multiplication rule for the composition of rotation variables, we can define the following rotation matrices used to pass to and from different reference frames.

$$\begin{aligned} \boldsymbol{R_b^n} &= \boldsymbol{R_k}(\psi) \times \boldsymbol{R_j}(\theta) \times \boldsymbol{R_i}(\phi) \\ \boldsymbol{R_b^n}^{\boldsymbol{T}} &= \boldsymbol{R_n^b} \end{aligned} \tag{2.4}$$

$$\begin{aligned} \boldsymbol{R_w^b} &= \boldsymbol{R_k}(\beta) \times \boldsymbol{R_j}(\alpha) \\ \boldsymbol{R_w^b}^{\boldsymbol{T}} &= \boldsymbol{R_b^w} \end{aligned} \tag{2.5}$$

$$\begin{aligned} \boldsymbol{R_b^p} &= \boldsymbol{R_j}(\mu) \\ \boldsymbol{R_b^p}^{\boldsymbol{T}} &= \boldsymbol{R_p^b} \end{aligned} \tag{2.6}$$

It must be noted that, if not specified, all vectors are considered in the body reference frame.

2.2 Atmospheric models

Different atmospheric models are used to emulate the various environments for the simulations. The objective is to provide enough complexity to the work, whilst also providing uniformity with other projects[4][8], as to allow for comparison of simulation and performance results.

2.2.1 Earth atmospheric model

Earth atmospheric density

In the model employed [9] for this project, the gravity is considered constant, at $g_E = 9.81[m/s^2]$. The temperature is modelled in segments, as to better approximate the different parts of earth's atmosphere [10].

$$\begin{aligned} &h > 25000\ [m] \\ &T = -131.21 + 0.00299h\ [^{\circ}C] \\ &p = 2.488\left[\frac{T+273.1}{216.6}\right]^{-11.388}\quad [kPa] \end{aligned} \tag{2.7}$$

$$\begin{aligned} 11000 < h &< 25000\ [m] \\ T &= -56.46\ [^circC] \\ p &= 22.65e^{(1.73-0.000157h)}\ [kPa] \end{aligned} \tag{2.8}$$

$$\begin{aligned} &h < 11000\ [m] \\ &T = 15.04 + 0.00649h\ [^{\circ}C] \\ &p = 101.29\left[\frac{T+273.1}{288.08}\right]^{5.256}\quad [kPa] \end{aligned} \tag{2.9}$$

Given the temperatures and pressures, the atmospheric density can be obtained as follows.

$$\rho = \frac{p}{0.2869(T+273.1)}\ [kg/m^3] \tag{2.10}$$

Earth wind model

Considering the parameters that describe the parafoil employed in the simulations on Earth[3], and the atmospheric characteristic of the planet itself, the system moves with a very low horizontal velocity. Hence it's capacity to reject wind disturbances is quite limited.
A possible approach for introducing a wind disturbance, that is both realistic and sustainable, is proposed. Taking the absolute value of the planar velocity relative to the atmosphere during a complete descent simulation, as shown in figure 2.3, we obtain a range of limit disturbance that the system is able to manage. Considering a fractional

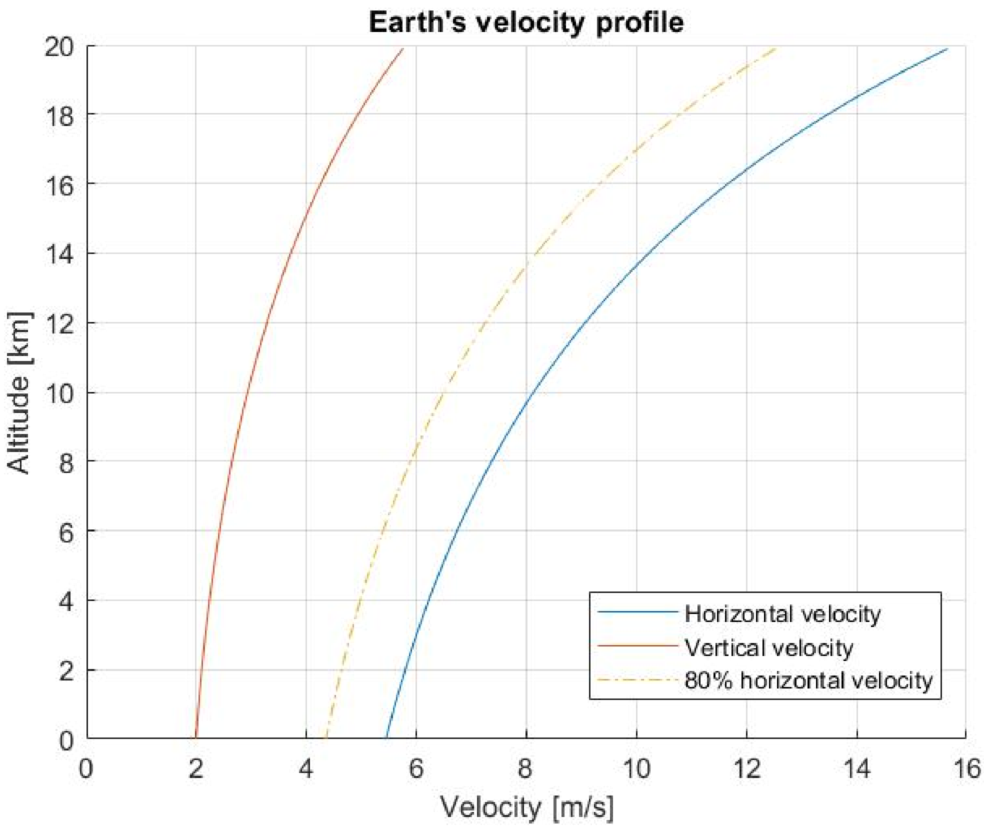

Figure 2.3: Earth's velocity profile

value, at each altitude, and using it in conjunction with a Gaussian distribution, we obtain a realistic yet manageable wind disturbance. This is similar to the approach taken in to account during the design of the actual parafoil[8], in order to evaluate it's ability to reject wind disturbances.

This approach doesn't reflect the real disturbances experienced by a parafoil, but allows performance analysis in case of severe disturbances, even with the small dimensions of the parafoil in question. The implementation in Simulink is done via a "look-up table".

2.2.2 Mars atmospheric model

Mars atmospheric density

Mars's ambient condition [11] present a very thin atmosphere, compared to Earth, and high gravity compared to Titan, $g_M = 3.7[m/s^2]$. As before, the temperature is modelled in segments, reflecting the different atmospheric layers, and the density is retrieved using the state equation for perfect gasses.

$$\begin{aligned} & h > 7000 \ [m] \\ & T = -23.4 - 0.00222h \ [°C] \\ & p = 0.699e^{-0.00009h} \ [kPa] \end{aligned} \tag{2.11}$$

$$\begin{aligned} & h < 7000 \ [m] \\ & T = -31 - 0.000998h \ [°C] \\ & p = 0.699e^{-0.00009h} \ [kPa] \end{aligned} \tag{2.12}$$

$$\rho = \frac{p}{0.1921(T + 273.1)} \ [kg/m^3] \tag{2.13}$$

Mars wind model

Considering the Gale Crater as the reference point for landing and averaging over the most favourable seasons, we obtain the following constant wind components.

$$\begin{aligned} & Wind\,in\,vertical\,direction : 2.3 \times 10^{-4} \, [m/s] \\ & Wind\,in\,South - North\,direction : 6.08 \, [m/s] \\ & Wind\,in\,West - East\,direction : 0.87 \, [m/s] \end{aligned} \tag{2.14}$$

Where the vertical component of the wind vector is negligible, the prevalent component blows from south to north, and a minor components blows in the east-west direction.
Albeit a crude approximation, it still is a significant representation of the ambient circumstances found on Mars, moreover it is aligned with other works [8].
In simulation, the values from (2.14) are used as central points of a Gaussian model for the wind disturbance.

2.2.3 Titan atmospheric model

Employing a similar approach as [4][6], the models describing the atmospheric density and wind magnitude are considered valid for possible landing sites of interest for future missions [12]. The acceleration of gravity is considered constant, where the mean value for titan is $g_T = 1.352 \ \ [m/s^2]$.

The exponential model for the atmospheric density (2.15) is taken from [13]. Although simple, it's still sufficient for the work at hand. Considering also the current utilization of the same model in other works cited here.

$$\rho(h) = 5.43e^{-5.1210^{-5}h}\ [kg/m^3] \tag{2.15}$$

The wind model model (2.16) is taken from [12][6]. It describes the magnitude of the major component of the wind disturbance, usually called the *Zonal Wind*, which blows from west to east. A minor component is also present in the north-south direction, the *Meridian wind*, which has a magnitude of $1 \div 2[m/s]$.

$$W_i(h) = \frac{W_{i,300}}{1 + e^{\frac{h_{i,0}-h}{L_i}}}\ \ [m/s] \tag{2.16}$$

In equation (2.16) the nominal parameters that best describe the ambient condition are $W_{i,300} = 22\ [m/s]$, $h_{i,0} = 35\ [km]$ and $L_i = 8\ [km]$.

2.3 System's mathematical models

Even though four and six degrees of freedom are usually considered low fidelity models[6], for our application and simulations they are more than sufficient. Also considering the fact that for this project, no specific payloads where taken in to account. Thus using only approximate information on payload dimensions and characteristics, which would lead to a futile analysis. Instead the following models are able to guarantee the needed level of detail, without being overly complex.

2.3.1 6 DoF parafoil model

A six degrees-of-freedom mathematical model was implemented from [3]. The model considers the parafoil and the payload as a single rigid body, thus simplifying the dynamics. The complete model is reported below.

Kinematics

The relevant velocities for the development of this work are: velocity relative to the ground $\boldsymbol{V}$; velocity relative to the air, $\boldsymbol{V_a}$; wind velocity,

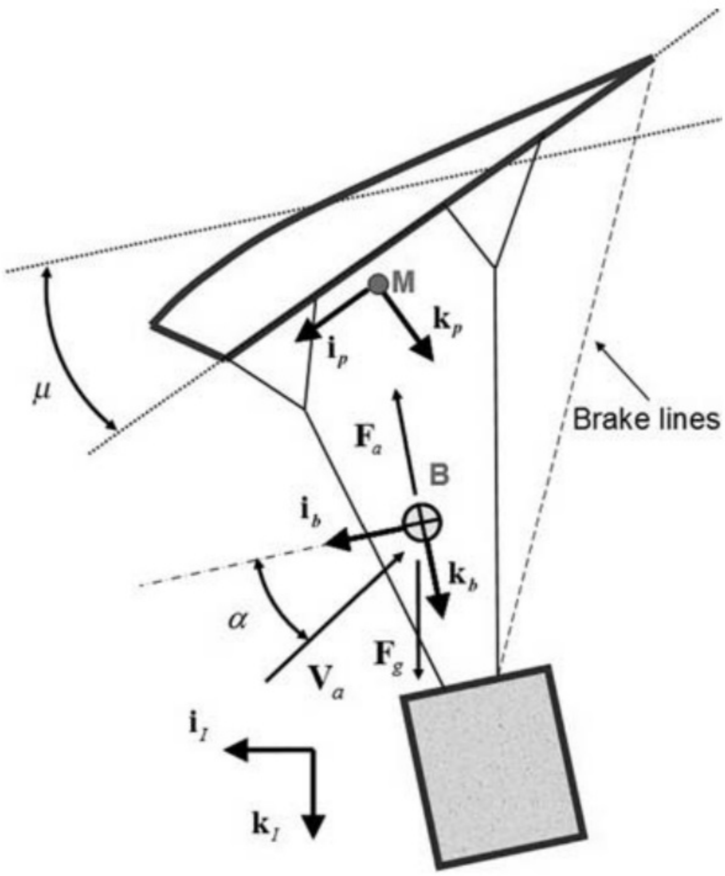

Figure 2.4: Parafoil's forces and reference frames

$\boldsymbol{W}$. The relation between this dimension is hereafter reported.

$$\boldsymbol{V_a} = \boldsymbol{V} + \boldsymbol{W} \tag{2.17}$$

Also, as per general definition, the main velocity components are listed below,

- Velocity relative to the atmosphere $\boldsymbol{V_a} = [v_x \ v_y \ v_z]^T$
- Ground speed vector in {b} $\boldsymbol{V} = [u \ v \ w]^T$
- Ground speed vector in {n} $\dot{\boldsymbol{p}} = [\dot{x} \ \dot{y} \ \dot{z}]^T$
- Angular velocity in {b} $\boldsymbol{\omega} = [p \ q \ r]^T$
- Angular velocity in {n} $\dot{\boldsymbol{\Phi}} = [\dot{\phi} \ \dot{\theta} \ \dot{\psi}]^T$

The transformation of the aforementioned velocities to the canopy reference frame can be done as follows.

$$\begin{bmatrix}\tilde{v}_x\\ \tilde{v}_y\\ \tilde{v}_z\end{bmatrix} = \boldsymbol{R_b^p}\left(\begin{bmatrix}u\\ v\\ w\end{bmatrix}\boldsymbol{S}(\boldsymbol{\omega})\begin{bmatrix}x_{BM}\\ y_{BM}\\ z_{BM}\end{bmatrix} - \boldsymbol{R_b^n W}\right)$$
$$\begin{bmatrix}\tilde{p}\\ \tilde{q}\\ \tilde{r}\end{bmatrix} = \boldsymbol{R_b^p}\begin{bmatrix}p\\ q\\ r\end{bmatrix} \tag{2.18}$$

Considering the angular velocities, we must define the kinematic transformation from {b} to {n},

$$[\boldsymbol{R_b^n}] = \begin{bmatrix}1 & \tan\theta\sin\phi & \tan\theta\cos\phi\\ 0 & \cos\phi & -\sin\phi\\ 0 & \frac{\sin\phi}{\cos\theta} & \frac{\cos\phi}{\cos\theta}\end{bmatrix}$$
$$[\boldsymbol{R_n^b}] = \begin{bmatrix}1 & 0 & -\sin\theta\\ 0 & \cos\phi & \sin\phi\cos\theta\\ 0 & -\sin\phi & \cos\phi\cos\theta\end{bmatrix} \tag{2.19}$$

Thus allowing for the relationship reported hereafter.

$$\boldsymbol{\omega} = [\boldsymbol{R_n^b}]\boldsymbol{\Phi} \quad \boldsymbol{\Phi} = [\boldsymbol{R_b^n}]\boldsymbol{\omega} \tag{2.20}$$

Apparent mass and inertia tensor

Given the dynamic characteristics, stemming from the inherent lightness of the system, the parafoil experiences a substantial influence from the atmosphere with which it interacts during flight. This interaction is not only found in the lift and drag aerodynamic forces, but also in the turbulent characteristics of the flow, which acts on the dynamics of the system[3][14].
This effect is modelled by the apparent terms of mass, inertia, forces and moments. This terms are approximations dependent on the physical characteristics of the system and the density of the fluid in which the system moves. Hereafter is the calculation of the apparent mass and inertia tensors.

$$a^* = \frac{a}{b} \quad and \quad t^* = \frac{t}{c} \tag{2.21}$$

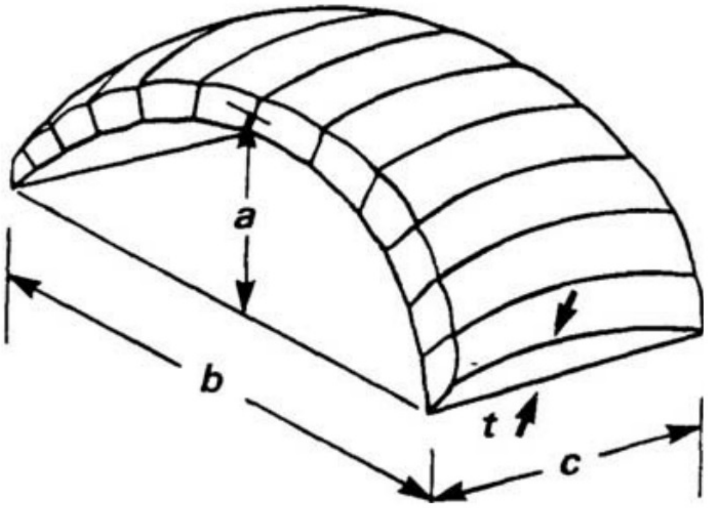

Figure 2.5: Canopy dimensions

$$\begin{aligned}
A &= 0.666\rho\left(1+\frac{8}{3}a^{*2}\right)t^2 b \\
B &= 0.267\rho\left[1+2\frac{a^{*2}}{t^{*2}}\mathrm{AR}^2\left(1-t^{*2}\right)\right]t^2 c \\
C &= 0.785\rho\sqrt{1+2a^{*2}\left(1-t^{*2}\right)}\frac{\mathrm{AR}}{1+\mathrm{AR}}c^2 b
\end{aligned} \tag{2.22}$$

$$\begin{aligned}
I_A &= 0.055\rho\frac{\mathrm{AR}}{1+\mathrm{AR}}c^2 b^3 \\
I_B &= 0.0308\rho\frac{\mathrm{AR}}{1+\mathrm{AR}}\left[1+\frac{\pi}{6}(1+\mathrm{AR})\mathrm{AR}a^{*2}t^{*2}\right]c^4 b \\
I_C &= 0.0555\rho\left(1+8a^{*2}\right)t^2 b^3
\end{aligned} \tag{2.23}$$

$$\boldsymbol{I_{a.m}} = \begin{bmatrix} A & 0 & 0 \\ 0 & B & 0 \\ 0 & 0 & C \end{bmatrix} \qquad \boldsymbol{I_{a.i}} = \begin{bmatrix} I_A & 0 & 0 \\ 0 & I_B & 0 \\ 0 & 0 & I_C \end{bmatrix} \tag{2.24}$$

In (2.24), the matrices are in the canopy reference frame, which is consistent with the following development of the apparent forces and moments. This components will then be expressed in the body reference frame (2.31)(2.32) to be employed in the dynamics equation (2.33).

Aerodynamic Forces and Moments

Forces acting on the parafoil are modelled in three macro components: apparent, aerodynamic and gravitational.

$$\begin{aligned} \boldsymbol{F_{ext}} &= \boldsymbol{F_a} + \boldsymbol{F_g} + \boldsymbol{F_{a.m}} \\ \boldsymbol{M_{ext}} &= \boldsymbol{M_a} + \boldsymbol{M_{a.i}} \end{aligned} \tag{2.25}$$

In (2.25), $\boldsymbol{F_a}$ is the aerodynamic force, $\boldsymbol{F_g}$ is the gravitational force and $\boldsymbol{F_{a.m}}$ is the force due to the apparent mass component. Also, $\boldsymbol{M_a}$ is the aerodynamic moment and $\boldsymbol{M_{i.a}}$ is the moment due to the apparent inertia.

$$\boldsymbol{F_g} = \begin{bmatrix} -\sin\theta \\ \cos\theta\sin\phi \\ \cos\theta\cos\phi \end{bmatrix} \tag{2.26}$$

$$\boldsymbol{F_a} = SQ\boldsymbol{R_w^b} \begin{bmatrix} C_{D0} + C_{D\alpha^2}\alpha^2 + C_{D\delta_s}\delta_s \\ C_{Y\beta}\beta \\ C_{L0} + C_{L\alpha}\alpha + C_{L\delta_s}\delta_s \end{bmatrix} \tag{2.27}$$

The aerodynamic moment expressed in {b} can be written as,

$$\boldsymbol{M_a} = SQ \begin{bmatrix} b\left(C_{l\beta}\beta + \frac{b}{2V_a}C_{lp}p + \frac{b}{2V_a}C_{lr}r + C_{l\delta_a}\delta_a\right) \\ \bar{c}\left(C_{m0} + C_{m\alpha}\alpha + \frac{c}{2V_a}C_{mq}q\right) \\ b\left(C_{n\beta}\beta + \frac{b}{2V_a}C_{nr}r + C_{n\delta_a}\delta_a\right) \end{bmatrix} \tag{2.28}$$

Apparent forces and moment

$$\boldsymbol{\tilde{F}_{a.m}} = -\left(\boldsymbol{I_{a.m}} \begin{bmatrix} \dot{\tilde{v}}_x \\ \dot{\tilde{v}}_y \\ \dot{\tilde{v}}_z \end{bmatrix} + \boldsymbol{S(\tilde{\omega})}\boldsymbol{I_{a.m}} \begin{bmatrix} \tilde{v}_x \\ \tilde{v}_y \\ \tilde{v}_z \end{bmatrix}\right) \tag{2.29}$$

$$\boldsymbol{\tilde{M}_{a.i}} = -\left(\boldsymbol{I_{a.m}} \begin{bmatrix} \dot{\tilde{p}} \\ \dot{\tilde{q}} \\ \dot{\tilde{r}} \end{bmatrix} + \boldsymbol{S(\tilde{\omega})}\boldsymbol{I_{a.i}} \begin{bmatrix} \tilde{p} \\ \tilde{q} \\ \tilde{r} \end{bmatrix} + \boldsymbol{S(\tilde{V}_a)}\boldsymbol{I_{a.m}} \begin{bmatrix} \tilde{v}_x \\ \tilde{v}_y \\ \tilde{v}_z \end{bmatrix}\right) \tag{2.30}$$

In equations (2.29) and (2.30) the components expressed with tilde (˜) are being expressed in the canopy reference frame and are acting on the apparent mass center. The apparent forces employ a definition of the velocities expressed in {p}(2.18). In order to use the the forces in the dynamic's equation of the body, all components must be projected in {b}.

$$\boldsymbol{F_{a.m}} = \boldsymbol{R_b^{pT}} \boldsymbol{\tilde{F}_{a.m}} \tag{2.31}$$

$$\boldsymbol{M_{a.i}} = \boldsymbol{R_b^{pT}} \boldsymbol{\tilde{M}_{a.i}} + \boldsymbol{S}(\boldsymbol{r}_{BM})\boldsymbol{F_{a.m}} \tag{2.32}$$

Where $\boldsymbol{r_{BM}} = [x_{BM}\ y_{BM}\ z_{BM}]^T$ is the vector from the system CoM to the apparent mass center. In our case we consider the simplification of it being coincident to the origin of the canopy reference frame. Also, $\boldsymbol{R_b^p}$ is a single axis transformation defined in (2.6).

Dynamics equation of motion

The final component to the model is the equations of motion (2.33), which consider all the forces and moments acting on the body, the masses and inertia, and allow for the calculation of the accelerations.

$$\begin{bmatrix} m_{tot}\boldsymbol{I_{3x3}} + \boldsymbol{I^*_{a.m}} & -\boldsymbol{I^*_{a.m}}\boldsymbol{S}(\boldsymbol{r}_{BM}) \\ \boldsymbol{S}(\boldsymbol{r}_{BM})I^*_{a.m} & \boldsymbol{I_p} + \boldsymbol{I^*_{a.i}} - \boldsymbol{S}(\boldsymbol{r}_{BM})\boldsymbol{I^*_{a.m}}\boldsymbol{S}(\boldsymbol{r}_{BM}) \end{bmatrix} \begin{bmatrix} \dot{u} \\ \dot{v} \\ \dot{w} \\ \dot{p} \\ \dot{q} \\ \dot{r} \end{bmatrix} = \begin{bmatrix} \boldsymbol{F_{ext}} \\ \boldsymbol{M_{ext}} \end{bmatrix} \tag{2.33}$$

This equation shall be integrated two times, in the simulation environment, to calculate the velocities and the position in space.

2.3.2 4 DoF parafoil model

The four degrees-of-freedom model is used int the MPC controller to approximate the time evolution of the system. It closely approximates the dynamics of the system, while remaining relatively computationally light.

Equation (2.34) describes the lift and drag components of the force affecting the parachute. In this approximation they're uncorrelated and depend only on symmetric input, systems characteristics, ambient condition and the module of the relative velocity with the atmosphere.

$$
\begin{aligned}
D &= QS\left(C_{D0} + C_{D\delta s}\delta_s\right) \\
L &= QS\left(C_{L0} + C_{L\delta s}\delta_s\right)
\end{aligned}
\tag{2.34}
$$

In (2.34), Q is called *Dynamic Pressure* and is defined as $\frac{\rho|V_a|^2}{2}$. It is the kinetic energy per unit volume of the fluid, an intrinsic characteristic of the moving fluid itself.
From (2.35) we obtain easily the dimension describing the parafoil interaction with the atmosphere.

$$
\begin{aligned}
|V_a| &= \sqrt{u^2 + w^2} \\
\alpha &= \tan^{-1}(\frac{w}{u})
\end{aligned}
\tag{2.35}
$$

The dynamics equation, obtained from [3], are hereafter reported.

$$
\begin{cases}
\dot{u} = \frac{L\sin\alpha - D\cos\alpha}{m} - w\dot{\psi}\sin\psi \\
\dot{\psi} = \frac{g\tan\phi}{u} + \frac{w\dot{\phi}}{u\cos\phi} \\
\dot{w} = \frac{-L\cos\alpha - D\sin\alpha}{m} + g\cos\phi + u\dot{\psi}\sin\phi \\
\dot{\phi} = \frac{1}{T_\phi}\left(-\phi + K_\phi\delta_a\right)
\end{cases}
\tag{2.36}
$$

The transition to the dynamics in the inertial reference frame(2.37), also referred to as the navigation equation.

$$
\begin{bmatrix} \dot{x} \\ \dot{y} \\ \dot{z} \end{bmatrix} = \boldsymbol{R_b^n} \begin{bmatrix} u \\ 0 \\ w \end{bmatrix}
\tag{2.37}
$$

It must be noted that the wind effect is not considered in this model. It is in fact a reduced order model that allows for lower a computational burden on the controller.

2.3.3 Stability

As noted in [3][6][5], the parafoil-payload system is an inherently stable system. Given the analysis carried out using the punctual linearization of the dynamic equations. Nonetheless the wind disturbance may cause difficulty in control when the magnitude of the disturbance approaches a significant fraction of the speed of the system. In this case, the controller which is ignorant of the wind component, seeing it only as a disturbance, faces difficulties in managing the differing response of the system.

2.3.4 Reduced order model parameters estimation

The reduced order model is used as an approximation of the system. The four degrees-of-freedom paradigm was chosen to allow for dual input, both symmetric and asymmetric. It is a nonlinear model, and thus provides a challenge for estimation purposes.
The choice of a grey-box model was made for reliability purposes. As it provides a higher physical interpretation of the approximated system.
The identification process employed consists of two phases, *data generation* and *parameters estimation*. The first deals with the fact that the data is obtained through means of simulation, hence it must be generated. The second is the actual estimation of the models parameters.
For a reliable estimation of the parameters, a point was made to employ data stemming from simulations witch used the actual controller. The reason is that it better represents the working conditions of the model and allows for longer simulation runs.

Initial set-up and data generation

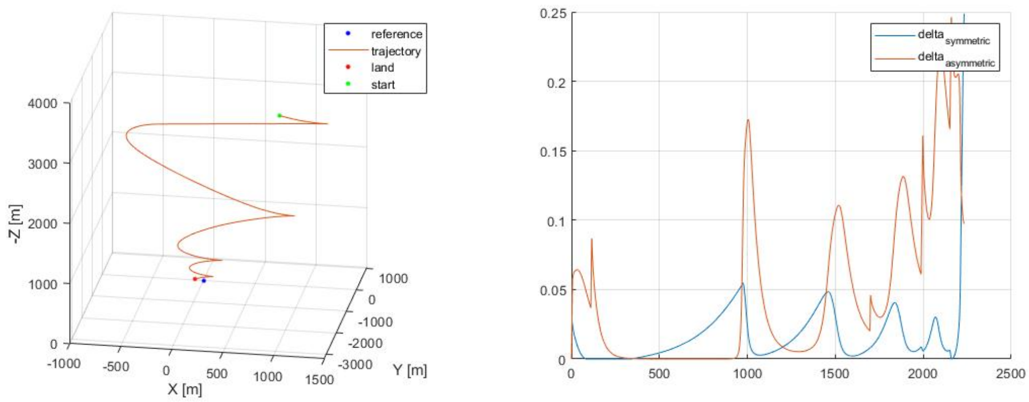

(a) Trajectory. (b) Control signal.

Figure 2.6: Example of simulation without wind, employed for parameters estimation.

Starting with a blank sheet, it is impossible to employ the controller to generate the data. A sufficient data-set is generated using a signal generator to excite the system.

The input signals used where step signals with different amplitudes. Exciting both the inputs, both separately and in unison. The objective was to try and cover as much of the operating conditions as possible. For stability of the simulation, most critically while employing a square input, the simulation step needed to be reduced. This highlighted the need for a sub-phase of the data generation process, post processing of the data-sets. Two techniques were used, decimation and segmentation.

Decimation of the data-set, effectively the post simulation reduction of the sampling frequency (from 1000 Hz or 100 Hz to 1 Hz), allowed to decrease the estimation time while increasing the quality; segmentation was tried to separate long simulation runs in shorter multi-run data-sets, which would better represent the prediction aspect of the controller, further specifying the ultimate utilization conditions of the model.

The data-sets generated where used in an initial round of the parameters estimation. This first parameters where used to include the controller in the simulations and generate more representative data-sets. Also in this case, post processing of the generated data-sets was needed.

Parameters estimation

The estimation is carried out using the non-linear grey box model parameters estimation function in Matlab[15]. Allowing for integrated handling of mathematical models, identification constraints, data-sets and search algorithms. A good degree of trial and error is needed to obtain a functional estimation of the model, which allowed and supported by the high flexibility and control worked in the function.

The final model employed in the controller, thus object of estimation, is reported in 3.2.1. In this case the parameters to be estimated are only those that describe the dynamics of the system, the atmospheric model uses an exact copy of what is already implemented to simulate the environment. In figure 2.7a2.7b is reported the comparison between the dynamics of the simulated system and that of the estimated model. It can be seen that even for long time frame, the estimated model are sufficiently close to the simulated system. It was also observed that, even if the estimated model is not perfectly approximating the system, the controller is able to perform sufficiently well. The estimated parameters are reported in appendix A.

2.3.5 Model selection for estimation

Selection of a model for estimation purposes is one of the most important tasks in order to succeed. Even more so when the system is non-linear. The choices, in this case, where limited by the decision of fitting a reduced order model of the dynamics to the generated data. Keeping in mind that the objective is to represent the dynamic behaviour of the system, the final goal is to drive the system towards the reference following a certain calculated path. The choice was thus made to use as output the position of the parafoil, considering the dynamics model augmented of the rotated kinematics (fig 3.1).
This solution yielded good results, ultimately being the choice throughout the development of this project. Still this field could greatly benefit form a further analysis on this point.

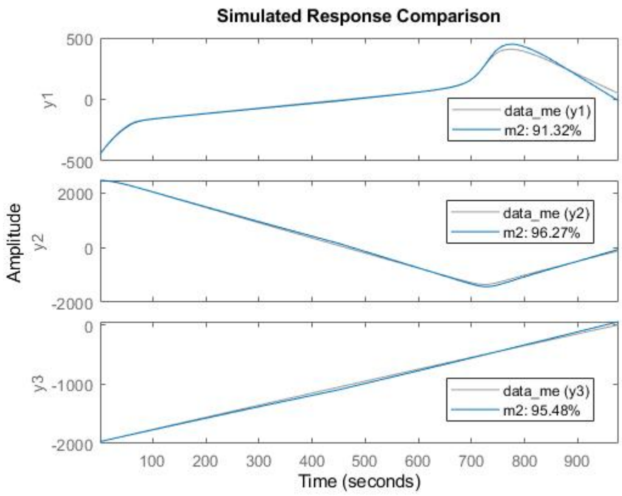

(a) Earth

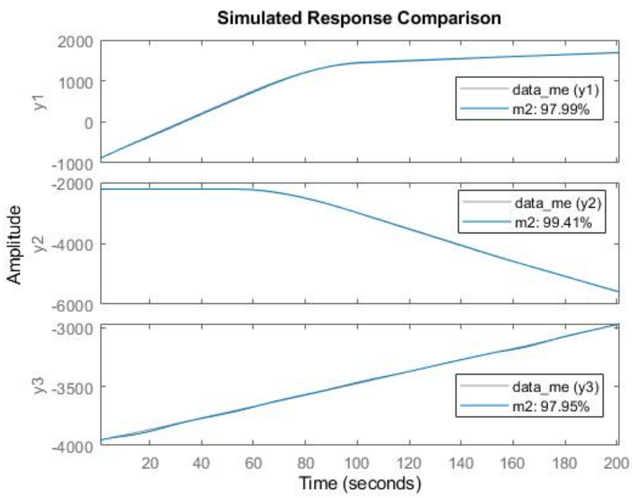

(b) Mars

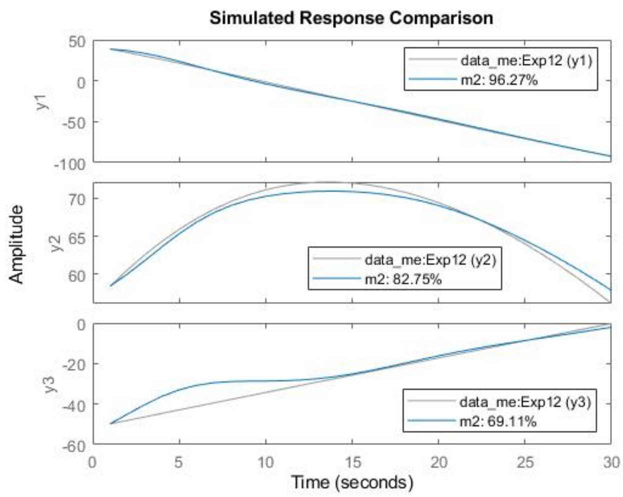

(c) Titan

Figure 2.7: Estimated model performance.

Chapter 3

Control design

A Model Predictive Controller (MPC) provides an intuitive approach to otherwise very difficult control problems. It is based on two steps, prediction and optimization. Prediction uses a model of the system to give the controller knowledge of the expected behaviour of the system, given it's initial conditions. Optimization is the decision component, where the controller optimises it's output in order to minimize a certain objective.
An nMPC provides an organic approach to the control solution, as it emulates the approach an operator would use in controlling a system. It is also very flexible in the applications, but it comes with the cost of high computational effort.

3.1 n-MPC controller

Considering a generic non-linear system defined below.

$$\begin{cases} \dot{x} & = f(x, u) \\ y & = h(x, u) \end{cases} \tag{3.1}$$

With states $x \in \mathbb{R}^n$, inputs $u \in \mathbb{R}^{n_u}$ and output $y \in \mathbb{R}^{n_y}$.
At each time $t = t_k$, the system is simulated in $[t, t + T_p]$. At any time $\tau \in [t, t + T_p]$, the predicted output $\hat{y}$ is a function of the initial state and the input signal $\hat{u}(t : \tau)$, which for now is a generic signal in the time interval $[t, \tau]$.

$$\hat{y}(\tau) \equiv \hat{y}(\tau, x(t), u(t, \tau)) \tag{3.2}$$

Thus at any time we look for an input signal which serves the objective of the control problem. This can be modelled considering the following objective function.

$$
J(\hat{u}(t:t+T_p)) = \int_t^{t+T_p} (\|\hat{e}(\tau)\|_Q^2 + \|\hat{u}(\tau)\|_R^2) d\tau + \|\hat{e}(t+T_p)\|_P^2
$$

$$
\begin{aligned}
\text{with} \quad & \hat{e}(\tau) = r(\tau) - \hat{y}(\tau) \\
& r(\tau) \in \mathbb{R}^{n_y} \\
& || \, . \, ||_X \; \text{ is the } \textit{weighted vector norm}
\end{aligned} \tag{3.3}
$$

Where the first term inside the integral is a cumulative reference tracking error, the second a cumulative controller effort, and the third a final tracking error. The weights in the vector norms are used to modify the effect that each vector component has on the final value of the objective function.
Then, the optimal control sequence $u^*(t : t{+}T_p)$ is obtained minimizing the objective function (3.3) under the following constraints.

$$
\begin{aligned}
& \dot{\hat{x}} = f(\hat{x}(\tau), \hat{u}(\tau)), \quad \hat{x}(t) = x(t) \\
& \hat{y} = h(\hat{x}(\tau), \hat{u}(\tau)) \\
& \tau \in [t, t+T_p]
\end{aligned} \tag{3.4}
$$

Up until this point, the control algorithm is in open loop. The controller simply takes the initial condition and evaluates the best strategy from that point on-wards, but doesn't take in to account any external disturbances or other uncertainties. This can be fixed using a sampling time, and thus the frequency at which the algorithm runs, that is sufficiently faster than the prediction horizon. This is called a *Receding Horizon* approach, and guarantees stability by emulating the effect that feedback has in conventional controllers[16].

3.2 n-MPC design

3.2.1 Prediction model of the parafoil system

The four degrees-of-freedom model (2.36), also called *reduced order* model, is employed for the prediction phase of the controller algorithm. Due to the high variation of atmospheric density during the descent, and the need for absolute positioning as an output for the controller, the model is augmented with (2.4) and the atmospheric models from section 2.2.

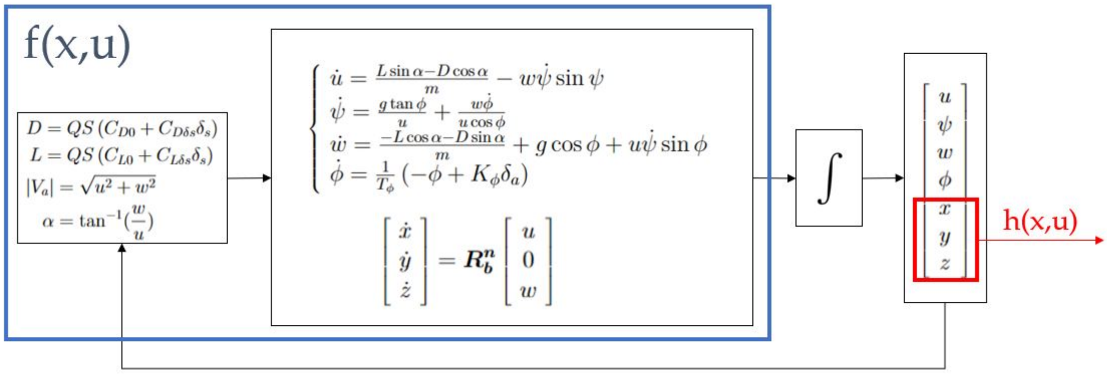

Figure 3.1: Prediction model scheme. In blue the dynamic equations of the system, defined as $f(x,u)$; in red the output function, defined as $h(x,u)$

In figure 3.1 a schematic representation of the prediction model. Inside of the nMPc, the f function is integrated with the *current step* condition and the calculated control input sequence. The h function in these application is the controlled output, which is simply the position of the system in $\{i\}$.

The presence of the atmospheric model inside the prediction model is made necessary by two factors, the approximation that is the reduced order model and the vertical span of the descents. The result is that if the atmospheric model is not considered, the controller would incur in errors resolving the initial condition. The altitude at which this problem arise is dependent on the estimation of the reduced order model parameters.

3.2.2 Optimization constraints

The constraints are used to guarantee that the calculated output is a physically realizable action. Thus two sets of constraints are used on the controlled input, scale and variation.

The scale constraint is tied to the mathematical modelization of the system, and depends on the fact that the inputs for the model are considered to be normalized. Thus, considering the definition for the controlled input, we obtain the following constraints.

$$u(\tau) = \begin{bmatrix}\delta_s\\ \delta_a\end{bmatrix}, \text{ with } \delta_a \in [0,1] \text{ and } \delta_s \in [-1,1] \tag{3.5}$$

The variation constraint limits the maximum variation, for the single vector components, from one time step to the next. It mainly serves two purposes, to limit chattering and avoid unreasonably large input variations that could lead to instability.

$$\|\delta(\tau) - \delta(\tau - T_s)\| \leq \Delta_{lim} \tag{3.6}$$

The constraints on the controlled input (3.5)(3.6) can thus be united considering directly a single limit, taking at any point the most stringent of the two conditions.

$$\begin{cases} \delta_{a_{max}} = min(1, \delta_a(\tau - T_s) + \Delta_{lim}) \\ \delta_{a_{min}} = max(0, \delta_a(\tau - T_s) - \Delta_{lim}) \end{cases}$$
$$\begin{cases} \delta_{s_{max}} = min(-1, \delta_s(\tau - T_s) + \Delta_{lim}) \\ \delta_{s_{min}} = max(1, \delta_s(\tau - T_s) - \Delta_{lim}) \end{cases} \tag{3.7}$$

3.2.3 Weight scheduling

The objective for the controller is to steer the system as close as possible to the desired landing site, which has already been established to be the origin in the {i} reference frame. In favor of lighter computation, no path planning algorithm is adopted. For this reason, the optimization weight for the cumulative tracking error is set to zero.
One peculiar complication of this approach is the difficulty of calibrating the optimization weight of P, Q and R for the desired behaviour. Since the path of the parafoil can span tens of kilometers, a constant weight ratio leads to varying performance characteristics along the descent.
To circumvent this effect, and to tune the behaviour of the system to mimic that of more complex approaches, the decision was made to implement *weight scheduling* on the controlled input term of optimization. Only one is sufficient, since the actual important part is the ratio between R and P. Fixing P equal to the identity matrix while varying R proved to work. Also adding Q with a very small multiplier, 0.1 or 0.001, resulted in much better performance in heavy wind conditions. Considering that the cause for the adverse behaviour of the controller was the massively spanning output of the system, the actual position in space, the weight scheduling is implemented as a function of the

norm of the controlled output vector [17]. The actual weight is set per intervals of this parameter.

$$
D_{WS} = \|p\| = \sqrt{x^2 + y^2 + z^2}
$$
$$
\begin{cases}
\text{if } D_{WS} \geq D_1 \rightarrow R = R_1 \\
\text{if } D_1 > D_{WS} \geq D_2 \rightarrow R = R_2 \\
\qquad\quad \vdots \\
\text{if } D_{n-1} > D_{WS} \geq D_n \rightarrow R = R_n \\
\text{if } D_n > D_{WS} \rightarrow R = R_{n+1}
\end{cases} \tag{3.8}
$$

In (3.8) is the compact explanation of the scheduler. This logic allows for easy implementation in the simulation environment, while providing a high degree of flexibility during tuning of the controller's parameters.
The tuning of the parameters was done by trial and error. Separating the descents in segments of interest and tuning segment by segment in until the desired behaviour was achieved. The parameters used for the scheduler are reported in appendix B.

Chapter 4

Simulation and results

In order to implement the models in Simulink, which was chosen as the simulation environment, the decision was made to utilize a block defined structure for all the forces and interacting components, instead of using a compact formulation of the model as presented in [3][8][4]. For more complex models, direct mathematical formulation should be used instead, as the faster simulation times are outweighted by the complexity of setting up and debugging the models.

The complete simulation environment, figure 4.1, is composed of five main blocks: external forces and moments, 6 DOF model for system's dynamics and equation of motion, atmospheric model, reduced order feedback, and the controller. At a macro level, the main inputs for the simulation are the initial conditions, such as absolute position in space, orientation and initial velocities, and the reference for the controller's objective.

The apparent components of weight and inertia are based on the geometry and aerodynamic characteristics of the system, but are ultimately proportional to the atmospheric density (2.24). The calculation of the fixed component is carried out during the set-up phase of the simulation, which is then multiplied with the atmospheric density in real time.

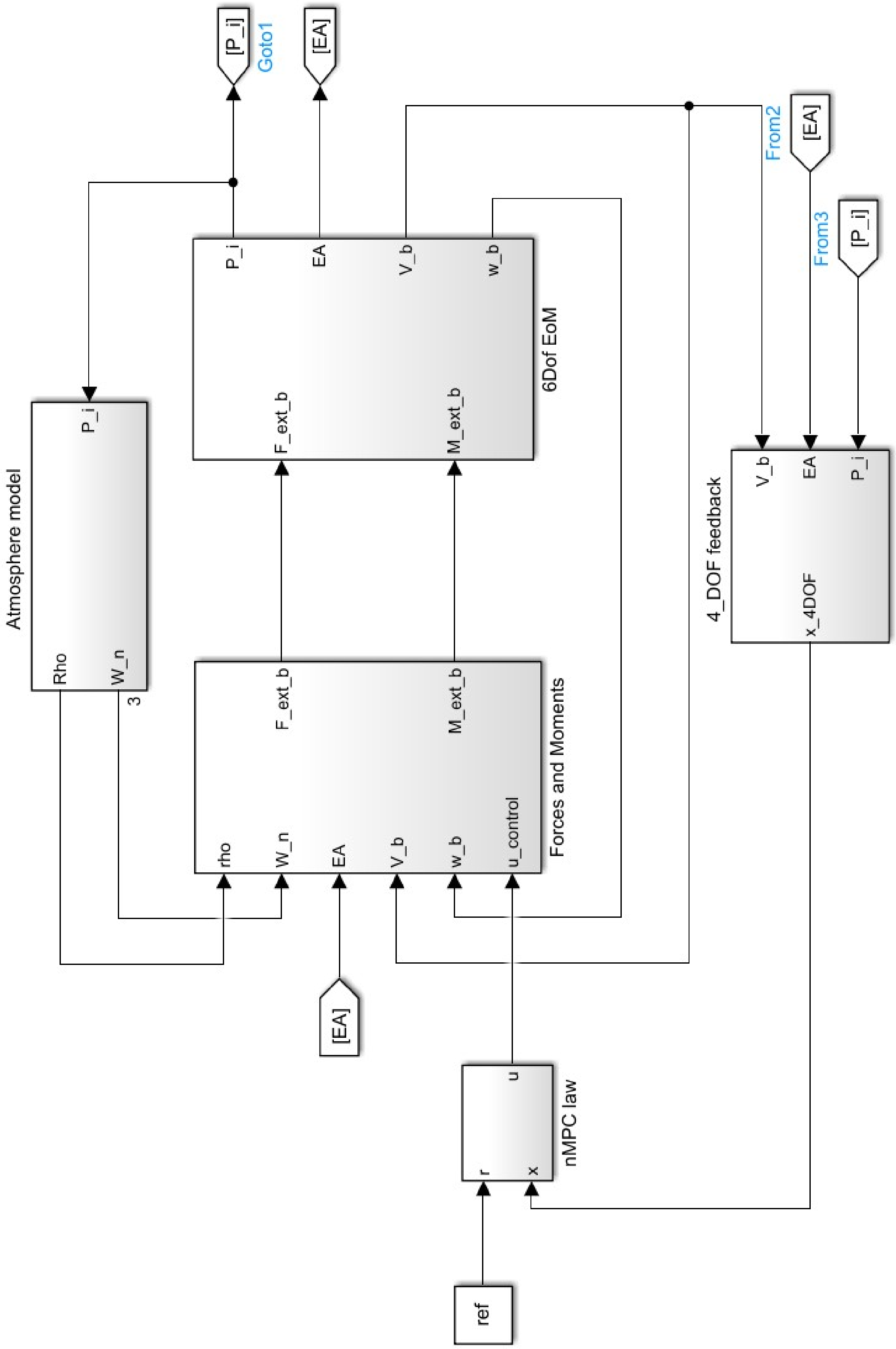

Figure 4.1: Complete simulation model.

4.1 Earth

The Monte Carlo simulation for Earh uses 300 runs, with the conditions reported below. Using randomly dispersed initial positions and wind directions allows to isolate the performance of the controller from the variability of the initial conditions.

1. Initial conditions
   (a) *Altitude* set at 10 km.
   (b) *Initial position* randomly chosen in a 30 km by 30 km square.
2. Wind generation
   (a) *Mean wind* as described subsection 2.2.3, with a wind fraction of 20%.
   (b) *Variance* for the additive gaussian distributed zero mean signal, set to 0.5 for the x direction and 0.05 for the y direction.
   (c) *Sampling time of random source* set to 1s.
3. Simulation environment parameters
   (a) *Termination condition* set for altitude equal to zero.
   (b) *Sampling time of the model* set to $10^{-2}s$.
   (c) *Sampling time data* set to 1s.
   (d) *Integration method:* ode4 (Runge-Kutta).

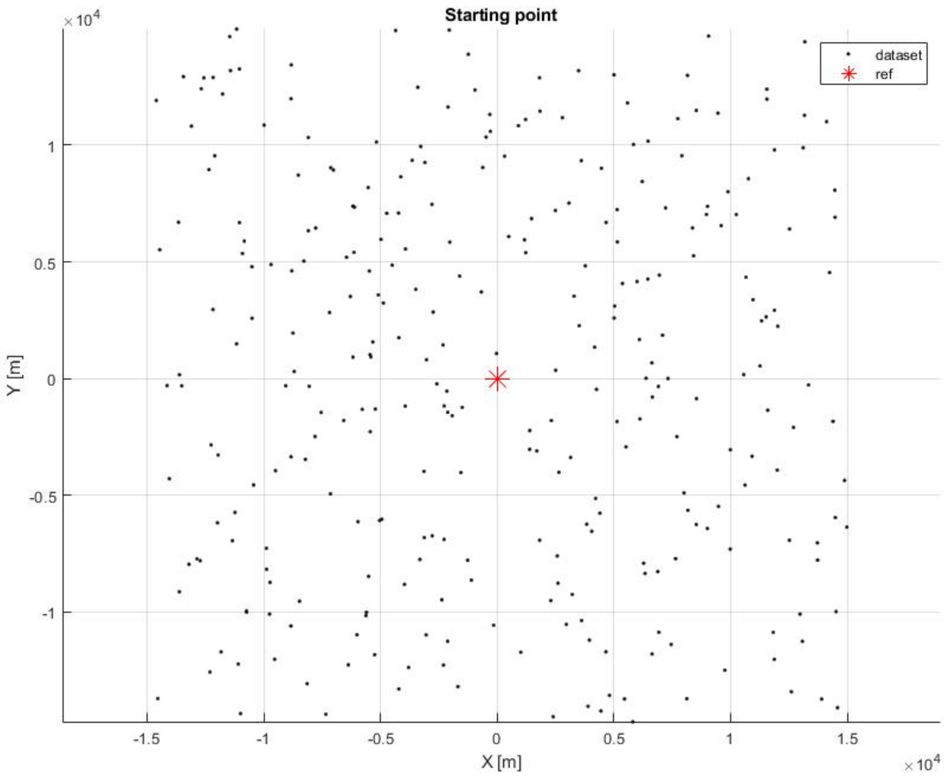

Figure 4.2: Simulations initial points at 10km altitude.

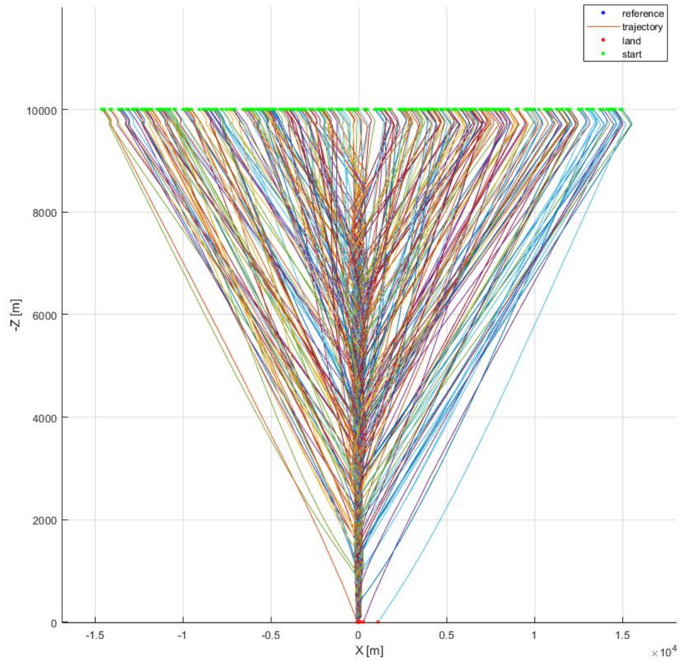

(a) X-Z Plane

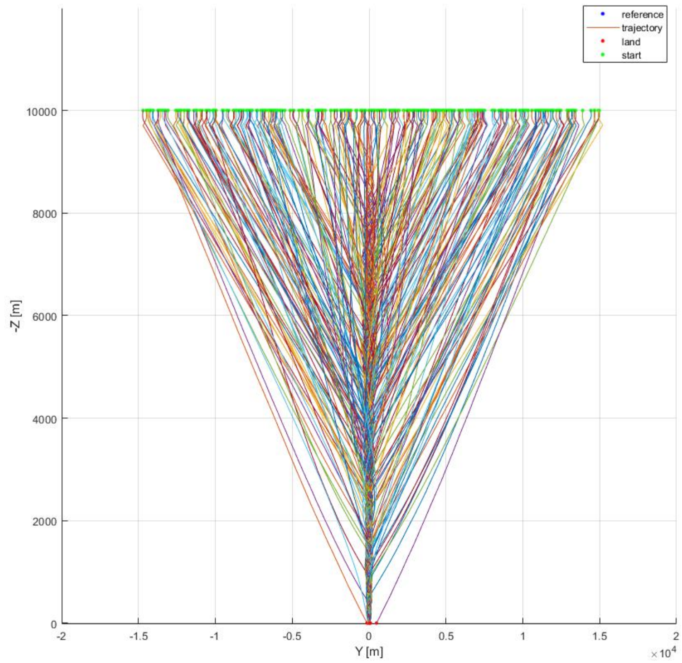

(b) Y-Z Plane

Figure 4.3: Earth Monte Carlo simulation trajectories.

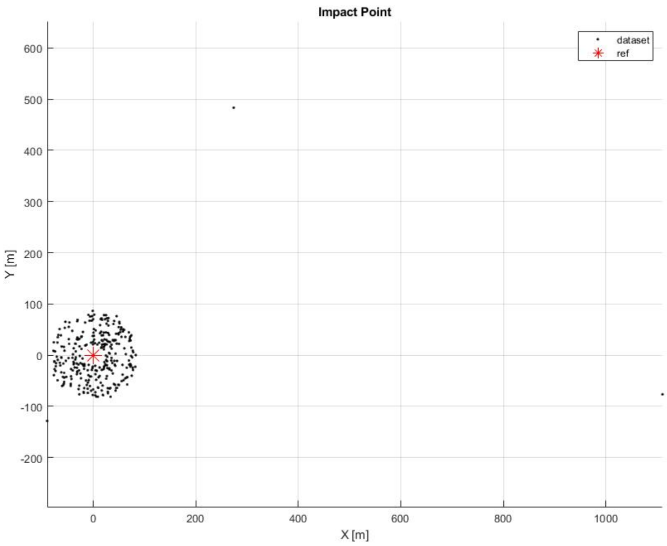

(a) Complete

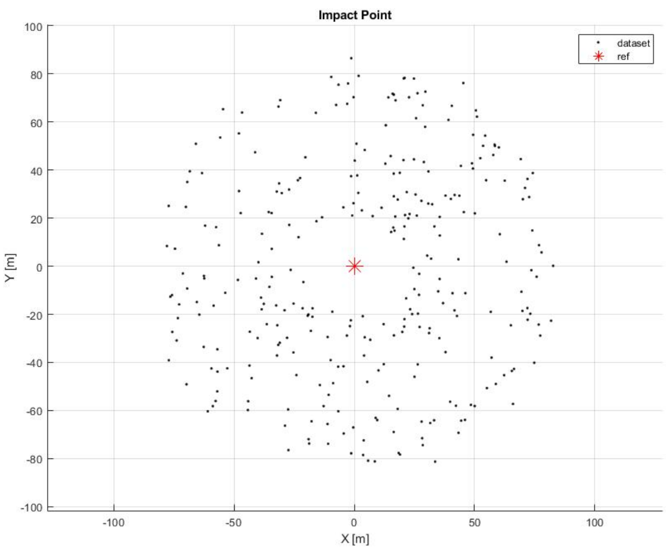

(b) Center focus

Figure 4.4: Earth Monte Carlo simulation impact points.

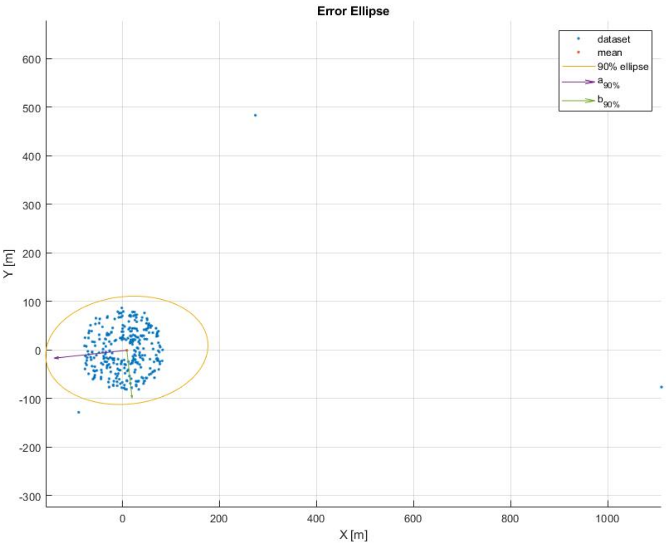

(a) Complete

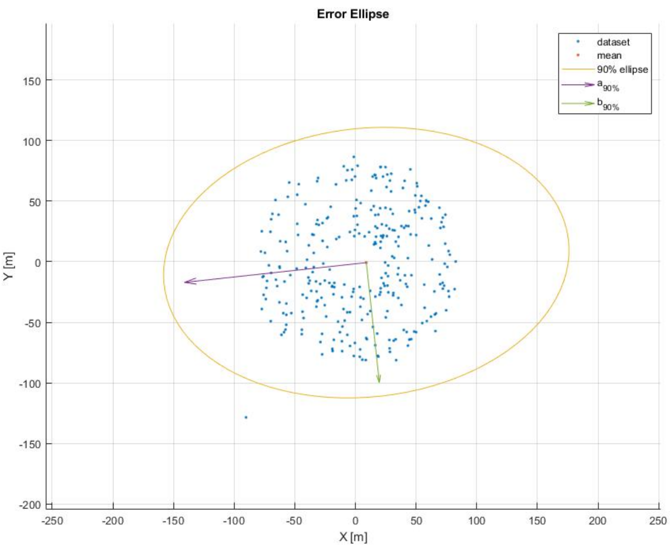

(b) Focus

Figure 4.5: Earth Monte Carlo simulation Error Ellipse for 90% confidence. The semi-major axis is 168 [m] long, the semi-minor axis is 111 [m] long.

4.2 Mars

The Monte Carlo simulation for Mars uses 300 runs, with the conditions reported below. Using randomly dispersed initial positions.

1. Initial conditions
   (a) *Altitude* set at 40 km.
   (b) *Initial position* randomly chosen in a 60 km by 60 km square.
2. Wind generation, figure 4.6
   (a) *Mean wind* as described subsection 2.2.2, a vector $W^n_{mean} = [6.08,\ 0.87,\ 0]^T$
   (b) *Variance* for the additive gaussian distributed zero mean signal, set to 0.5 for the x direction and 0.05 for the y direction.
   (c) *Sampling time of random source* set to $5s$.
3. Simulation environment parameters
   (a) *Termination condition* set for altitude equal to zero.
   (b) *Sampling time of the model* set to $10^{-2}s$.
   (c) *Sampling time data* set to $1s$.
   (d) *Integration method:* ode4 (Runge-Kutta).

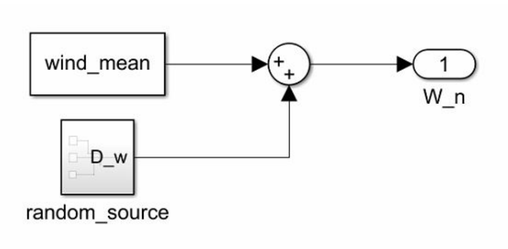

(a) Wind generation block.

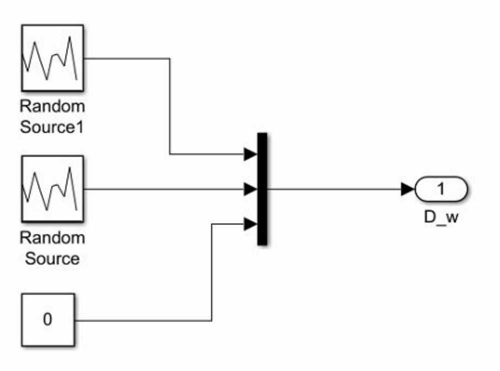

(b) Random source block.

Figure 4.6: Wind generation for Mars simulation.

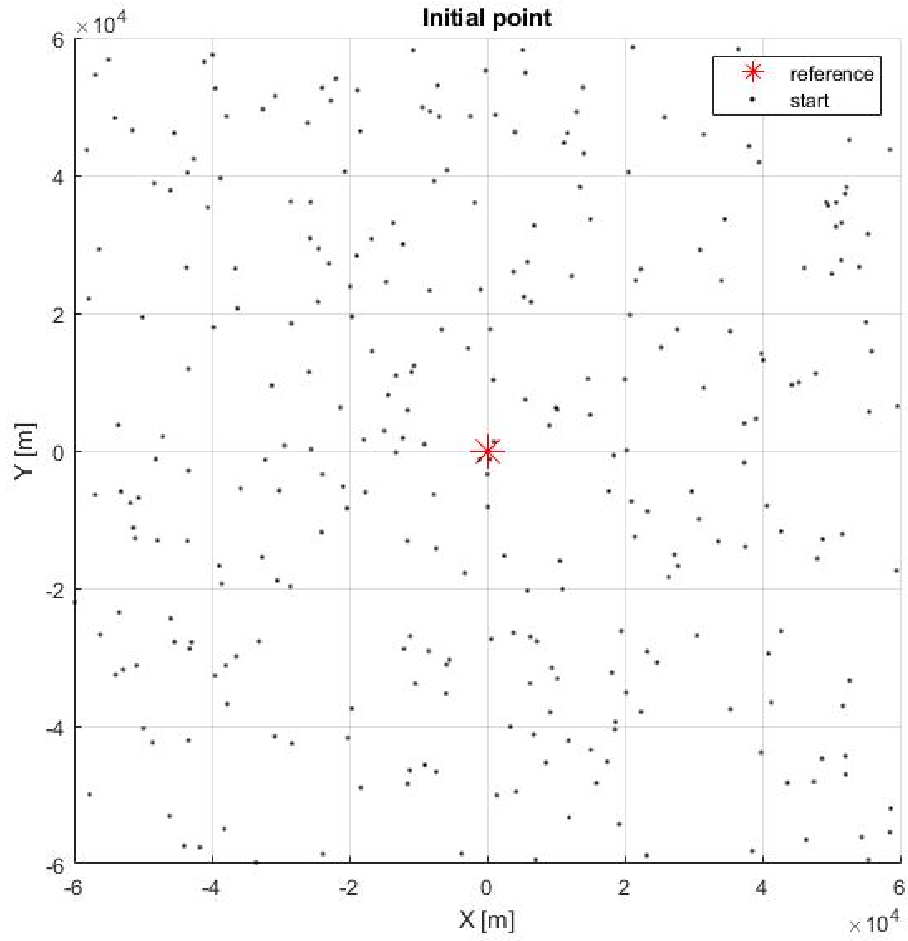

Figure 4.7: Simulations initial points at 40km altitude.

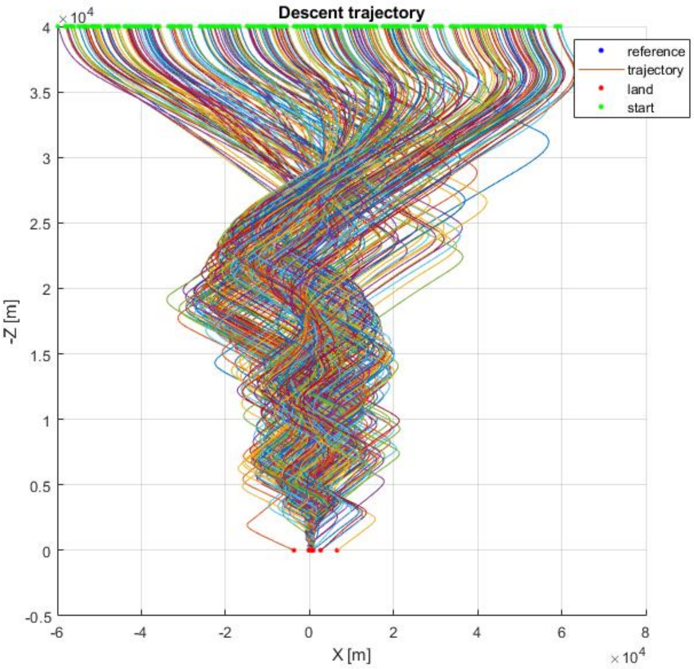

(a) X-Z Plane

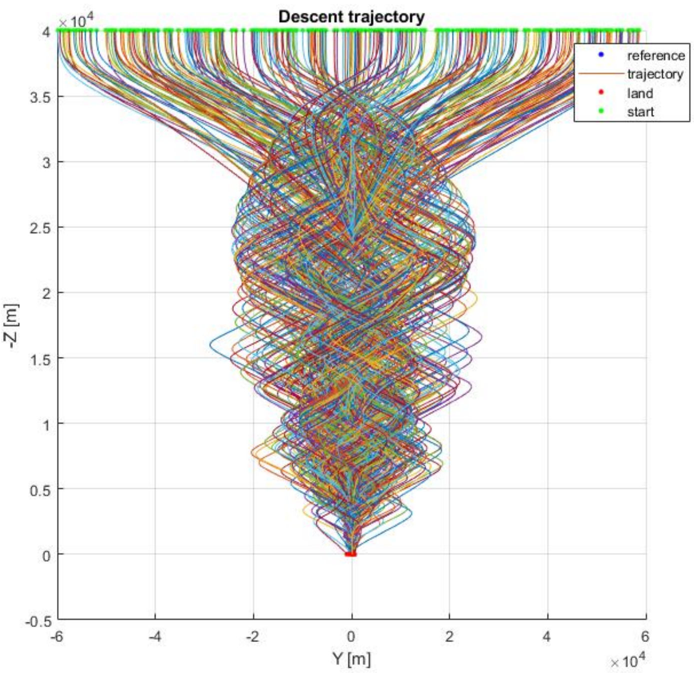

(b) Y-Z Plane

Figure 4.8: Mars Monte Carlo simulation trajectories.

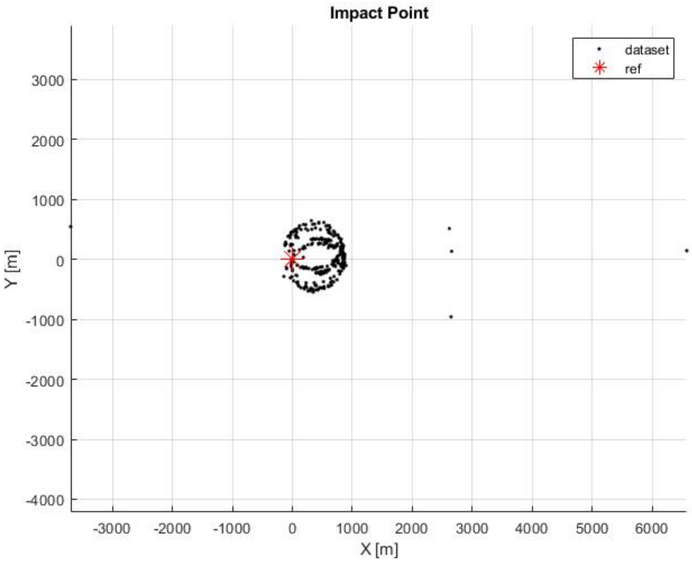

(a) Complete

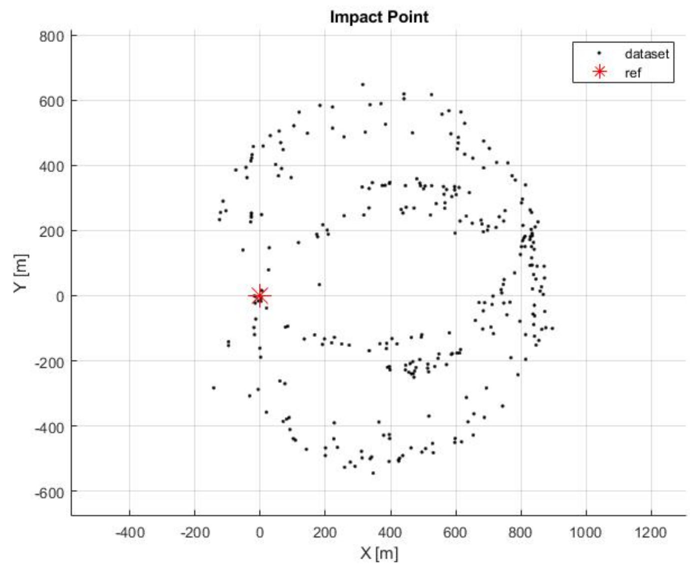

(b) Center focus

Figure 4.9: Mars Monte Carlo simulation impact points.

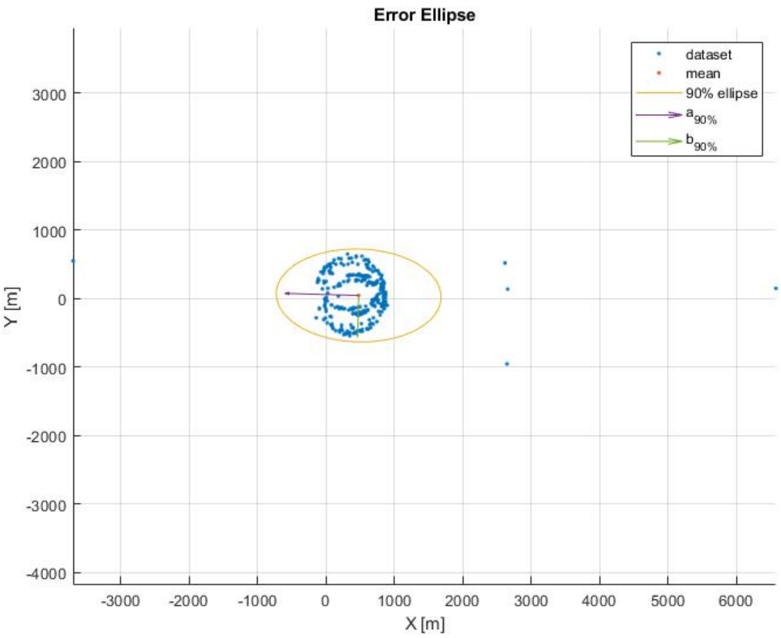

(a) Complete

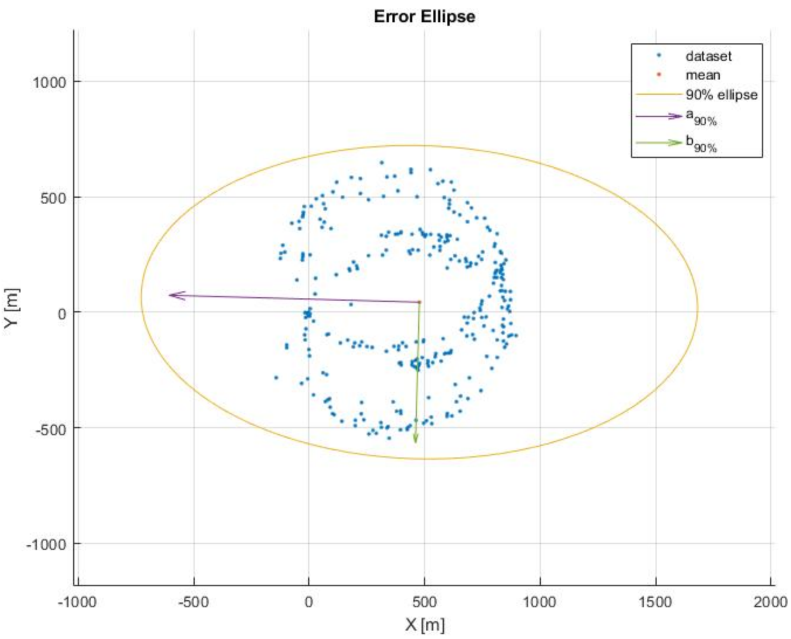

(b) Focus

Figure 4.10: Mars Monte Carlo simulation Error Ellipse for 90% confidence. The semi-major axis 1.205 km long, the semi-minor axis is 678 long.

4.3 Titan

The Monte Carlo simulation for Titan uses 300 runs, with the conditions reported below. Using randomly dispersed initial positions.

1. Initial conditions
   (a) *Altitude* set at 40 km.
   (b) *Initial position* randomly chosen in a 120 km by 120 km square.
2. Wind generation
   (a) *Mean wind* as described subsection 2.2.3, $W_{i,300} = 8\ [m/s]$, $h_{i,0} = 35\ [km]$ and $L_i = 8\ [km]$.
   (b) *Variance* for the additive gaussian distributed zero mean signal, set to 0.1 for the *Zonal* wind and 0.01 for the *Meridian* wind.
   (c) *Sampling time of random source* set to $1s$.
3. Simulation environment parameters
   (a) *Termination condition* set for altitude equal to zero.
   (b) *Sampling time of the model* set to $10^{-2}s$.
   (c) *Sampling time data* set to $1s$.
   (d) *Integration method:* ode4 (Runge-Kutta).

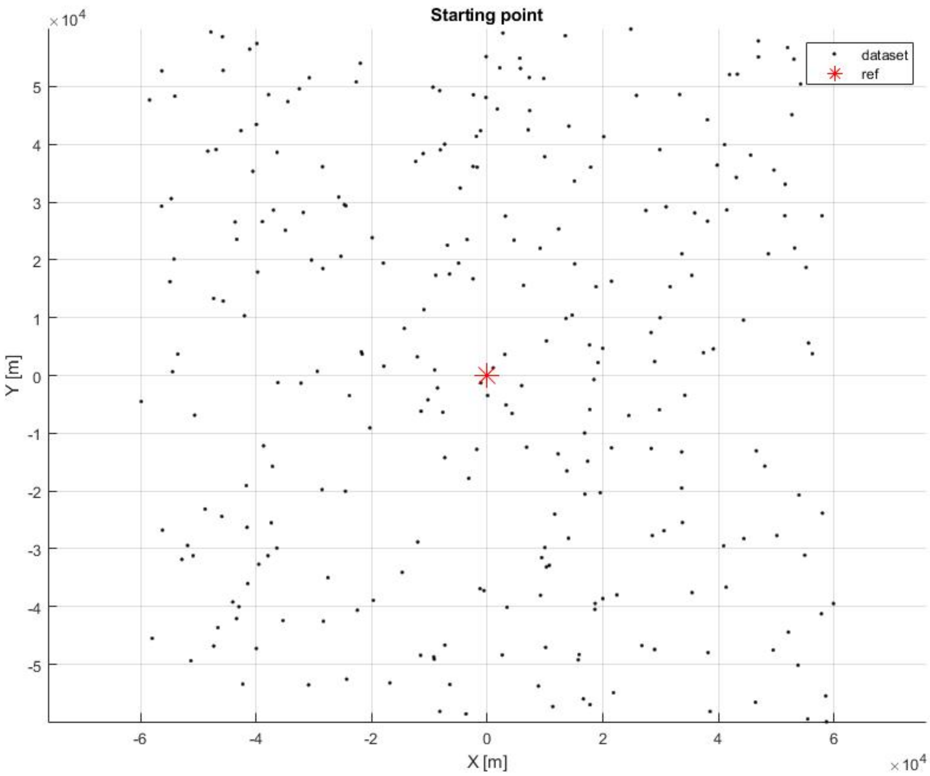

Figure 4.11: Simulations initial points at 40km altitude.

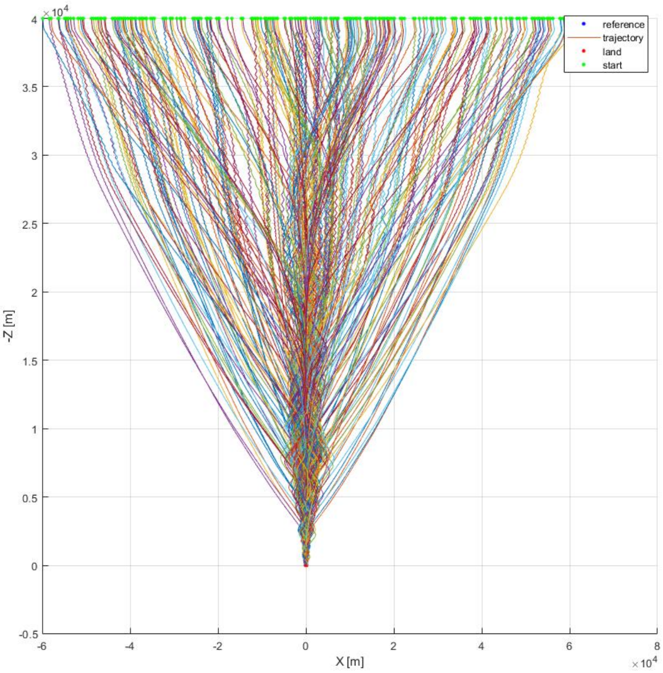

(a) X-Z Plane

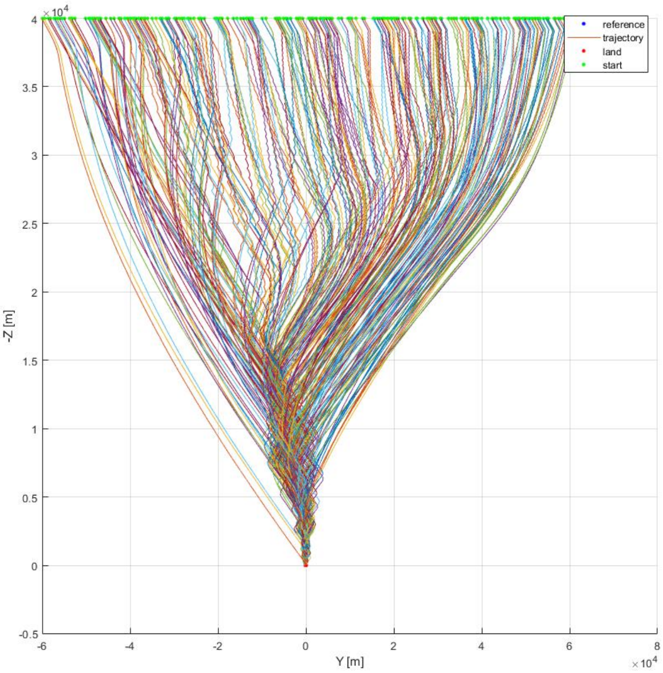

(b) Y-Z Plane

Figure 4.12: Titan Monte Carlo simulation trajectories.

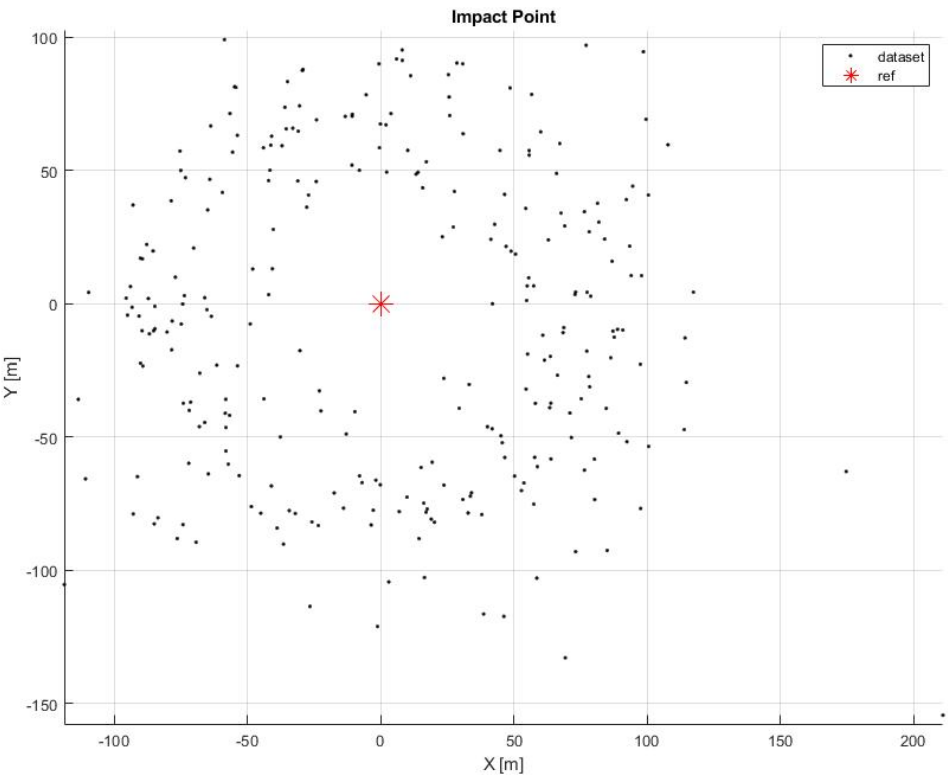

Figure 4.13: Titan Monte Carlo simulation impact points.

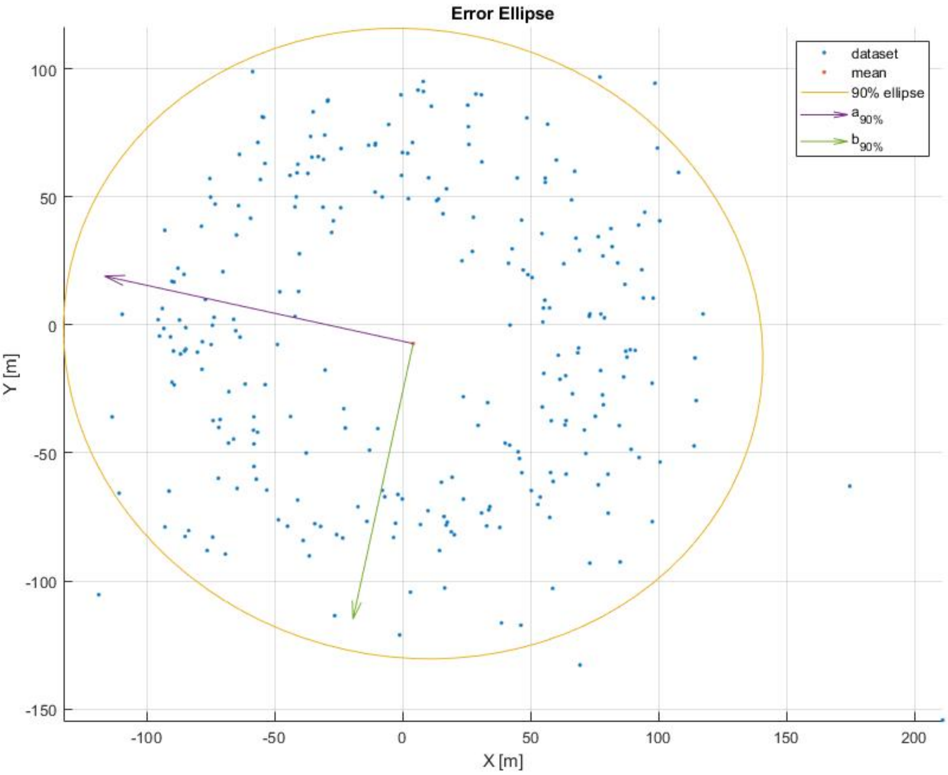

Figure 4.14: Titan Monte Carlo simulation Error Ellipse for 90% confidence. The semi-major axis 2.546 km long, the semi-minor axis is 1.382 km long.

4.4 Simulations results

During the simulations several critical aspects where highlighted, from the different behaviours due to the differences in the atmospheric conditions, to the instabilities that wind can bring to the system behaviour. Hereafter is a review of the main conclusions.

4.4.1 Wind instability and correlation to performance

Taking as example the simulations on earth, at high altitudes and high wind conditions, it can be observed how the controller struggles to maintain the calculated course for the system. A comparison between this phenomena and the nominal behaviour can be seen in figure 4.15. In the unstable conditions, the optimal trajectory calculated by the controller is significantly different from time step to time step. This behaviour comes with extremely high chattering of the controllers output.
Reducing the wind component almost negates this behaviour. In this case, the system is able to follow the calculated course and the controller output is smooth and punctual.
From observation of this phenomena, it can be ascribed to the faster dynamics of the system when going upwind. The behaviour is also due to the treatment of the wind only as a disturbance that is not taken in to account by the controller.
Depending on how the wind model is implemented in the simulation environment, and how it varies during the descent, this behaviour can have increasingly detrimental effects on the final performance of the controller. The singular effect of this instability can't be separated from the simple disturbance of the wind, as it is a product of the disturbance itself. In figure 4.16 we can observe the variation of the landing dispersion for increasing values of mean wind speeds.

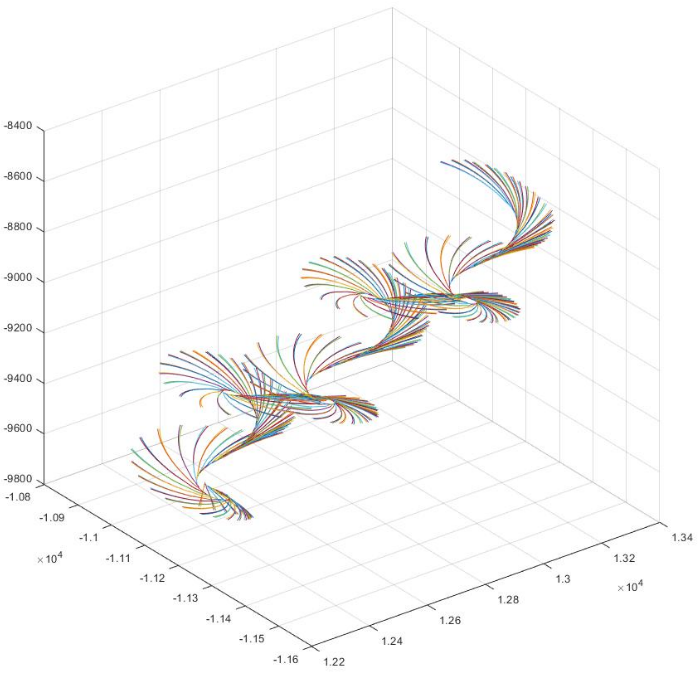

(a) Unstable conditions

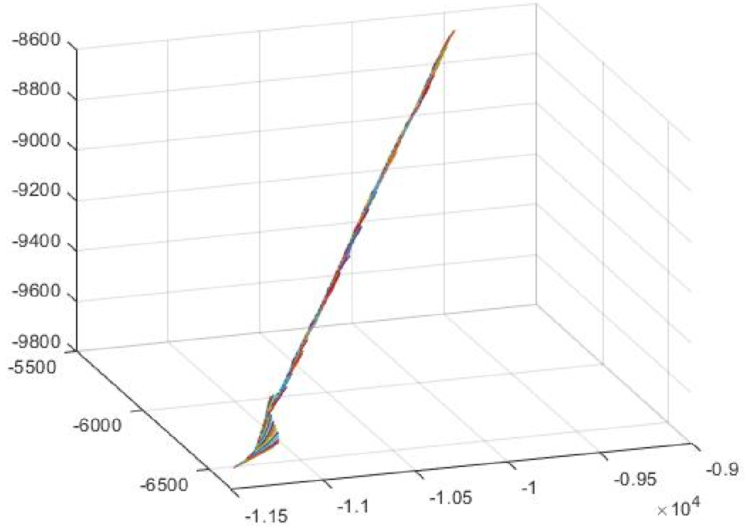

(b) Stable conditions

Figure 4.15: Comparison between unstable, figure (a), and stable conditions, figure(b). The simulation is carried out in Earth's environment at 10 km altitude. Wind fractions are 30% for the unstable condition and 3% for the stable conditions.

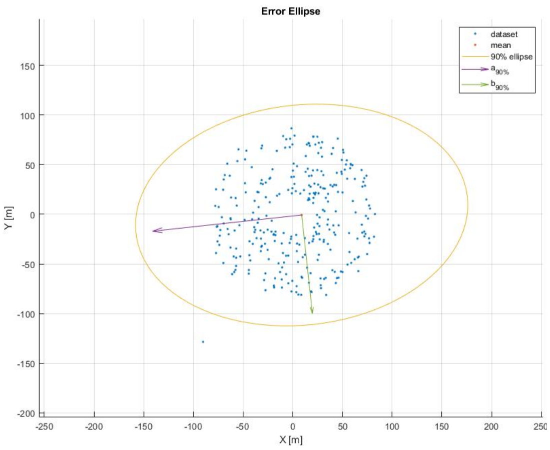

(a) 20% wind, semi-major axis 168 m, semi-minor axis 111 m.

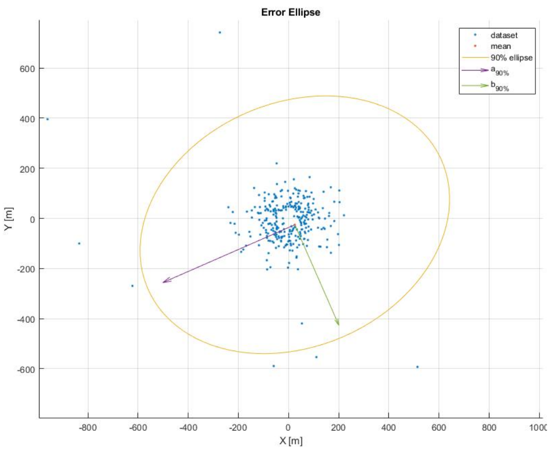

(b) 30% wind, semi-major axis 639 m, semi-minor axis 486 m.

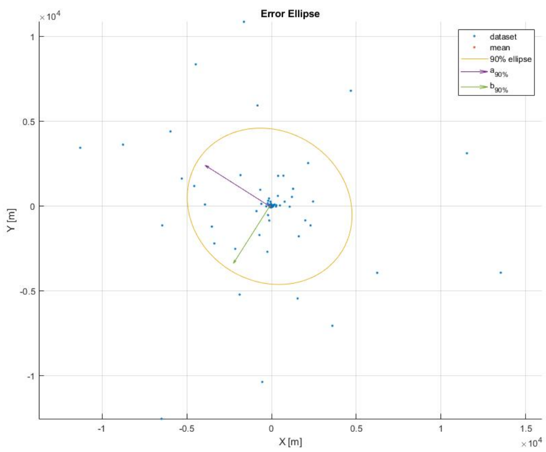

(c) 45% wind, semi-major axis 5.02 km, semi-minor axis 4.44 km.

Figure 4.16: Comparison of landing accuracy for increasingly high mean wind speeds. Simulations carried out in Earth's environment with the same controller parameters. Wind direction and initial position are random, with each mean wind speed was being simulated 300 times. Percentages associated to the mean wind speed are relative to the planar/horizontal velocity at each altitude.

4.4.2 Controller parameters tuning, effects and behaviour

The parameters that define the behaviour of an MPC are virtually infinite, given all the possible variations on how the control problem is stated. Considering the formulation employed for this project, the following parameters where selected as being of most interest.

- $\boldsymbol{P}$ weight of the final error weighted norm. Set constant, equal to identity matrix.
- $\boldsymbol{Q}$ weight of the cumulative error weighted norm, it's presence drastically improved the behaviour in high wind conditions, allowing for better tracking of the calculated trajectory.
- $\boldsymbol{R}$ weight of the cumulative control effort weighted norm. As reported in (3.8), this matrix is scheduled based on the norm of the position vector in the inertial reference frame. The tuning was done to regulate the control effort during the descent, reducing chattering and promoting long passes with intermittent turns over spiraling. This is accomplished tuning high values at high distances and proportionally lower values as the system gets to the intended landing point. A balance has to be struck between the intended behaviour and the attractivity of the origin, as if the parameter is set too high, the controller looses authority.
- $\boldsymbol{T_{prediction}}$ is the prediction horizon of the controller. From the beginning it was set at 20 seconds, or 20 time intervals, as it struck a good balance between prediction and computing complexity.
- $\boldsymbol{T_{sample}}$ is the duration of the time intervals. It is set at 1 second, as in all other studies of this type.
- $\boldsymbol{T_{control}}$ is the calibrated time after which the controller starts working. It is effective in allowing the system to settle in it's steady state condition at the beginning of the simulation. This parameter can be set to anything between 40 and 100 second, in the applications considered in this work. In principle, this parameter should allow the oscillations that may arise at the beginning of the simulation to disappear, while not removing too much time from the controller to effectively steer the system towards the intended landing point.

4.4.3 General performance of the controller

Many factors concur to the final performance of the controller, from the identification of the reduced order models parameters, the tuning of the controller, to the atmospheric conditions. In all cases, the results of the simulations show how the controller is able to correctly perform under generally nominal atmospheric conditions (see figures 4.5, 4.10 and 4.14). Considering the dispersion of the landing points as a bi-variate gaussian distribution, the values of the semi-axis of the error ellipses calculated for a 90% likelihood are comparable with other works done in the field [18][8][4].
One of the reasons for employing weight scheduling techniques in the control problem, was to favour straight descents with intermittent turns. Avoiding spiraling trajectories, which are less favourable from a landing speed perspective. The trajectories are not spiraling downwards (see figures 4.3, 4.8 and 4.12), but appear more as a vertical triangular line. On Mars, where the horizontal velocity is highest, and the wind disturbance is lowest, this behaviour is more easily observed.

Chapter 5

Conclusions

This thesis aims at demonstrating the applicability of this control strategy to different environments. Augmenting the base strategy of the model predictive controller with the scheduling of the optimization weights, allows the system to respond in a more tunable and flexible fashion, while not adding computational complexity to the control problem.

The use of autonomous parafoil systems is widely considered in many descent application, from the logistics of payload delivering to planetary exploration. High lift coefficients in modern designs have significantly broadened the possible applications of this solutions. Still limitations remain, mainly given by limited maneuverability and implication that high wind disturbance have on the final operating range. Thus the ability to navigate the environment depends on the atmospheric and wind conditions, and not only on the system itself. Suggesting that a high degree of planning is needed to guarantee success in hostile environments.

To realize what stated above, a simulation environment was developed in Simulink, encompassing a 6 degrees-of-freedom model of the system, atmospheric conditions for the different planetary applications, variable wind disturbances and initial conditions. The simulation environment was used both in the estimation of the reduced order model parameters, and in the Monte Carlo simulations for the evaluation of the performance of the controller.

Specifically, the project was carried out along the following topics:

- **Study and implementation of the dynamic model of the parafoil system.** While implementing in a simulation environment the dynamic equations of a system is usually a straight for-

ward endeavour, in the case of parafoil system a lot of incomplete information is found in literature. Thus a lot of time was initially spent on finding a complete model and all the relative parameters to correctly describe the system. The six degrees-of-freedom model was chosen to describe the dynamics, as it is found in many different works. Allowing for a simple simulation framework that can be employed in all the different planetary applications.
For the prediction model, the four dof model was chosen above a three dof model. The choice is motivated by the dual input of the first, compared to the single input of the latter. Allowing for further flexibility in the control of the system.

- **Identification of the reduced order model parameters** required a lot of trial and error. A methodology was developed to obtain valid data, whilst considering the computational complexity that this problem poses. The final results are far from perfect, from a numerical stand-point, but yield sufficiently good performance in the simulations, evidence of the flexibility of the control strategy employed.

- **Development and tuning of the final n-MPC controller.** The base formulation of the non-linear Model Predictive Controller was taken from previous works, but demonstrated to be non-robust and insufficiently adaptable to the problem at hand. The scheduling of the optimization weight pertaining to the control effort, previously found only in wind turbines, proved to be highly effective at tackling the numerical variance of the input variables of the objective function.

As a next step, further works should focus on:

- Employ an estimator for the wind disturbance, a Kalman filter using a suitable linearization of the reduced order model, to add the wind in the prediction calculations of the controller. This could also be used in a more complete simulation where sensor noise is considered on the systems variables.

- High fidelity models, nine degrees of freedom, would allow the analysis on the influence of the oscillation of the payload on the controllers performance and consider a more accurate description of the aerodynamic behaviour.

- Stretch the simulation to include the whole entry and descent phase, for planetary exploration applications. Considering the multiple phases of a mission of this type.

Appendix A

Parameters of mathematical models

A.1 Parameters for Earth

System′s physical parameters		
m_{tot}	2.4	kg
J	$diag[0.42 \;\; 0.4 \;\; 0.053]$	$kg\, m^2$
S	1	m^2
μ	-12	deg
$r_{_{BM}}$	$[0.046 \;\; 0 \;\; -1.11]^T$	m
a	0	m
b	1.35	m
c	0.75	m
t	0.075	m

Reduced order model parameters		
C_{L0}	0.8189	–
$C_{L\delta_s}$	0	–
C_{D0}	0.2919	–
$C_{D\delta_s}$	0	–
K_ϕ	0.3802	rad
T_ϕ	5	s

System's aerodynamic parameters		
Aerodynamic force coefficients		
C_{D0}	0.25	–
$C_{D\alpha^2}$	0.12	rad^{-2}
$C_{D\delta_s}$	0.3	–
C_{Yb}	-0.23	rad^{-1}
C_{L0}	0.091	–
$C_{L\alpha}$	0.9	rad^{-1}
$C_{L\delta_s}$	0.21	–
Aerodynamic moment coefficients		
$C_{l\beta}$	-0.036	rad^{-1}
C_{lp}	-0.84	rad^{-1}
C_{lr}	-0.082	rad^{-1}
$C_{l\delta_a}$	-0.0035	–
C_{m0}	0.35	–
$C_{m\alpha}$	-0.72	rad^{-1}
C_{mq}	-1.49	rad^{-1}
$C_{n\beta}$	-0.0015	rad^{-1}
C_{np}	-0.082	rad^{-1}
C_{nr}	-0.27	rad^{-1}
$C_{n\delta_a}$	0.0115	–

A.2 Parameters for Mars

System's physical parameters		
m_{tot}	13.685	kg
J	$diag[3.76\ \ 3.02\ \ 0.418]$	$kg\, m^2$
S	14	m^2
μ	-12	deg
$r_{_{BM}}$	$[0\ \ 0\ \ -5.05]^T$	m
ϵ	35.8	rad
a	0	m
b	6.48	m
c	2.16	m
t	5.18	m

Reduced order model parameters		
C_{L0}	0.8606	$-$
$C_{L\delta_s}$	2.808	$-$
C_{D0}	0.1579	$-$
$C_{D\delta_s}$	0.1331	$-$
K_ϕ	-0.5425	rad
T_ϕ	0.9604	s

System's aerodynamic parameters		
Aerodynamic force coefficients		
C_{D0}	0.078	$-$
$C_{D\alpha^2}$	0	rad^{-2}
$C_{D\delta_s}$	0.08	$-$
C_{Yb}	-0.23	rad^{-1}
$C_{Y\delta_a}$	-0.0096	$-$
C_{L0}	0.4066	$-$
$C_{L\alpha}$	3.1672	rad^{-1}
$C_{L\delta_s}$	0.13	$-$
Aerodynamic moment coefficients		
$C_{l\beta}$	-0.24	rad^{-1}
C_{lp}	-4.5	rad^{-1}
C_{lr}	-0.8	rad^{-1}
$C_{l\delta_a}$	-0.252	$-$
C_{m0}	0	$-$
$C_{m\alpha}$	-0.615	rad^{-1}
C_{mq}	-0.182	rad^{-1}
$C_{n\beta}$	0.16	rad^{-1}
C_{np}	-0.8	rad^{-1}
C_{nr}	-0.16	rad^{-1}
$C_{n\delta_a}$	-0.04	$-$

A.3 Parameters for Titan

System's physical parameters		
m_{tot}	200	kg
J	$diag[11.9267\ \ 3\ \ 1.667]$	$kg\,m^2$
S	3.14	m^2
μ	-12	deg
$r_{_{BM}}$	$[0.26\ \ 0\ \ -1.5]^T$	m
a	0.164	m
b	3.072	m
c	1.023	m
t	0.075	m

Reduced order model parameters		
C_{L0}	0.6105	$-$
$C_{L\delta_s}$	0.1440	$-$
C_{D0}	0.2897	$-$
$C_{D\delta_s}$	0.0965	$-$
K_ϕ	1.0483	rad
T_ϕ	0.6673	s

System′s aerodynamic parameters		
Aerodynamic force coefficients		
C_{D0}	0.25	–
$C_{D\alpha^2}$	0.12	rad^{-2}
$C_{D\delta_s}$	0.1	–
C_{Yb}	-0.23	rad^{-1}
$C_{Y\delta_a}$	0	–
C_{L0}	0.091	–
$C_{L\alpha}$	0.9	rad^{-1}
$C_{L\delta_s}$	0.15	–
Aerodynamic moment coefficients		
$C_{l\beta}$	-0.0036	rad^{-1}
C_{lp}	-0.84	rad^{-1}
C_{lr}	-0.082	rad^{-1}
$C_{l\delta_a}$	-0.0035	–
C_{m0}	0.35	–
$C_{m\alpha}$	-0.72	rad^{-1}
C_{mq}	-1.49	rad^{-1}
$C_{n\beta}$	-0.0015	rad^{-1}
C_{np}	-0.082	rad^{-1}
C_{nr}	-0.27	rad^{-1}
$C_{n\delta_a}$	0.0115	–

Appendix B

Parameter of n-MPC controller

B.1 Parameters for Earth

Controller's base parameters	
$\boldsymbol{P}$	$\boldsymbol{I_3}$
$\boldsymbol{Q}$	$\boldsymbol{I_3}$
T_p	20
T_{start}	50
T_s	1

Scheduled intervals for R	
$h > 10km$	$850\boldsymbol{I_2}$
$10km \geq h > 7km$	$650\boldsymbol{I_2}$
$7km \geq h > 5km$	$550\boldsymbol{I_2}$
$5km \geq h > 3km$	$450\boldsymbol{I_2}$
$3km \geq h > 1km$	$350\boldsymbol{I_2}$
$1km \geq h > 500m$	$300\boldsymbol{I_2}$
$500m \geq h > 200m$	$250\boldsymbol{I_2}$
$h \leq 200m$	$150\boldsymbol{I_2}$

B.2 Parameters for Mars

Controller's base parameters	
$\boldsymbol{P}$	$\boldsymbol{I_3}$
$\boldsymbol{Q}$	$\sim$
T_p	20
T_{start}	100
T_s	1

Scheduled intervals for R	
$h > 10km$	$500\boldsymbol{I_2}$
$10km \geq h > 7km$	$400\boldsymbol{I_2}$
$7km \geq h > 5km$	$300\boldsymbol{I_2}$
$5km \geq h > 3km$	$110\boldsymbol{I_2}$
$3km \geq h > 1km$	$80\boldsymbol{I_2}$
$1km \geq h > 500m$	$40\boldsymbol{I_2}$
$500m \geq h > 200m$	$5\boldsymbol{I_2}$
$h \leq 200m$	$\boldsymbol{I_2}$

B.3 Parameters for Titan

Controller's base parameters	
$\boldsymbol{P}$	$\boldsymbol{I_3}$
$\boldsymbol{Q}$	$0.01\boldsymbol{I_3}$
T_p	20
T_{start}	100
T_s	1

Scheduled intervals for R	
$h > 10km$	$600\boldsymbol{I_2}$
$20km \geq h > 10km$	$500\boldsymbol{I_2}$
$10km \geq h > 7km$	$400\boldsymbol{I_2}$
$7km \geq h > 5km$	$300\boldsymbol{I_2}$
$5km \geq h > 3km$	$200\boldsymbol{I_2}$
$3km \geq h > 1km$	$100\boldsymbol{I_2}$
$1km \geq h > 500m$	$80\boldsymbol{I_2}$
$500m \geq h > 200m$	$30\boldsymbol{I_2}$
$h \leq 200m$	$20\boldsymbol{I_2}$

Bibliography

[1] Bobby Kazeminejad, David H. Atkinson, Miguel Pérez-Ayúcar, Jean-Pierre Lebreton, and Claudio Sollazzo. Huygens' entry and descent through titan's atmosphere—methodology and results of the trajectory reconstruction. *Planetary and Space Science*, 55(13):1845–1876, 2007. Titan as seen from Huygens. 5

[2] Oleg Yakimenko, Vladimir Dobrokhodov, James Johnson, Isaac Kaminer, Scott Dellicker, and Richard Benney. *On Control of Autonomous Circular Parachutes*. 6

[3] Oleg A Yakimenko. *Precision aerial delivery systems : modeling, dynamics, and control*. American Institute of Aeronautics and Astronautics, Inc., 2015. 6, 12, 13, 14, 17, 19, 23, 33

[4] Giacomo Bonaccorsi. Dynamic Programming and ModelPredictive Control Approach for Autonomous Landings. *Journa of Guidance, Control and Dynamics*, 2022. 6, 13, 16, 33, 54

[5] Wolf White and Dean F. A theory of three-dimensional parachute dynamic stability. *Journal of Aircraft*, 5(1):86–92, 1968. 6, 23

[6] Jasmine Rimani. High lift systems for planetary descent and landing, 2018-10-23. 6, 13, 16, 17, 23

[7] Michael B. Ward, Mark Costello, Jacob Wachlin, Benjamin Leon, Keith Bergeron, and Gregory Noetscher. *Jumper-Inspired Guidance Logic for Precision Guided Airdrop Systems*. 6

[8] Alessandro Mercurio. Design and modeling of an autonomous parafoil for rover mars landing, 2021-04-13. 13, 15, 16, 33, 54

[9] NASA. Earth atmosphere model. `https://www.grc.nasa.gov/www/k-12/airplane/atmosmet.html`. 14

[10] Wikipedia. Atmosphere of earth. `https://en.wikipedia.org/wiki/Atmosphere_of_Earth`. 14

[11] NASA. Mars atmosphere model. https://www.grc.nasa.gov/www/k-12/airplane/atmosmrm.html. 15

[12] Ralph D. Lorenz, Claire E. Newman, Tetsuya Tokano, Jonathan L. Mitchell, Benjamin Charnay, Sebastien Lebonnois, and Richard K. Achterberg. Formulation of a wind specification for titan late polar summer exploration. *Planetary and Space Science*, 70(1):73–83, 2012. 16, 17

[13] Roger V. Yelle, D. F. Strobell, Emmanuel Lellouch, and Daniel Gautier. Engineering models for titan's atmosphere, 1998. 17

[14] P. LISSAMAN and GLEN BROWN. Apparent mass effects on parafoil dynamics. 19

[15] MathWorks. Estimate nonlinear grey-box model parameters. https://it.mathworks.com/help/ident/ref/nlgreyest.html. 25

[16] Carlo Novara. Course notes for non-linear control and aerospace application, 2021-2022. 29

[17] Thorben Wintermeyer-Kallen, Sebastian Dickler, János Zierath, Thomas Konrad, and Dirk Abel. Weight-scheduling for linear time-variant model predictive wind turbine control toward field testing. *Forschung im Ingenieurwesen*, 85(2):385–394, 2021. 32

[18] Robert M. Manning Robert D. Braun. Mars exploration entry, descent, and landing challenges. *Journal of Spacecraft and Rockets*, 44(2), March-April 2007. 54